sediment transport in rivers

flow of water in a curved open channel with a fixed plane bed

H. J. de Vriend and F.G. Koch

report on experimental and theoretical investigations

R 657-V
M 1415 part I

Oktober 1977

toegepast onderzoek waterstaat

CONTENTS

LIST OF TABLES

LIST OF FIGURES

LIST OF SYMBOLS

a	Maximum error in the measured flow angle due to the backlash in the keyway
A	Cross-sectional area
B	Channel width
c_1	Slope of the calibration curve of the velocity meter
c_2	Value of the velocity corresponding to zero measured frequency of pulses
c_{2_0}	Value of c_2 at calibration temperature
c_3	Rating coefficient of the direction meter
c_4	Coefficient of proportionality in the temperature correction term of c_2
C	Chézy's roughness factor
C_1	Calibrated value of c_1
d	Characteristic depth of flow
dC_1	Error in C_1
dZ	Error in Z_i for $i > 1$
dZ_1	Error in Z_1
$d\phi'_k$	Error in the measured flow angle due to the backlash in the keyway
$f=N/T$	Mean frequency of pulses counted during a velocity measurement
Fr	Froude number
g	Acceleration due to gravity
h	Local depth of flow
h_7	Depth of flow in the channel axis
H	Measured local depth of flow
$\bar{h}(E_0)$	Depth of flow averaged over cross-section E_0
i	Number of the grid point ($i = 1$ near the bed)
n	Number of pulses to be counted by the velocity meter during an observation
N	Number of pulses counted by the velocity meter during an observation
np	Number of grid points in a vertical
Q	Discharge
R	Local radius of curvature
R_c	Radius of curvature of the channel axis
Re	Reynolds number
T	Duration of the observation period for a velocity measurement
$temp_c$	Water temperature during the calibration of the velocity meter
$temp_m$	Water temperature during the measurements

LIST OF SYMBOLS (continuation)

$\bar{v}$	Mean velocity
v_{hel}	Local time-mean helical velocity component
v'_{hel}	Normalized helical velocity component
v_{main}	Local time-mean main velocity component
v'_{main}	Normalized main velocity component
v_r	Local time-mean radial velocity component
$\bar{v}_r$	Depth-averaged value of v_r
v_t	Local time-mean tangential velocity component
$\bar{v}_t$	Depth-averaged value of v_t
v_{tot}	Local time-mean total velocity
$\bar{v}_{tot}$	Magnitude of the depth-averaged velocity vector
z	Vertical distance to the bed
z_b	Bed level ($z_b = 0$ in the straight section)
z_s	Water surface elevation (datum: bed in the straight section)
$\bar{z}_s$	Water surface elevation averaged over the relevant cross-section
Z_i	Measured vertical distance of the grid point i to the bed
α	Direction of the depth-averaged velocity vector
η	Dynamic viscosity of the fluid
η_0	Dynamic viscosity of the fluid during calibration of the velocity meter
κ	Von Kármán's constant
μ_{dC_1}	Mean of dC_1
ν	Kinematic viscosity of the fluid
σ_{dC_1}	Standard deviation of dC_1
σ_{dZ}	Standard deviation of dZ
σ_{dZ_1}	Standard deviation of dZ_1
σ_H	Standard deviation of the error in H
$\sigma_{\Phi'_0}$	Standard deviation of the error in Φ'_0
ϕ	Local time-mean flow angle
ϕ'	Local time-mean flow angle to be measured by the direction meter
ϕ'_0	True reference angle of the direction meter
Φ'	Measured local time-mean flow angle
Φ'_0	Measured reference angle of the direction meter

SUMMARY

In this report the flow of water in a curved open channel, which consists of a 38 m long straight section followed by a 90^{o} bend with a radius of curvature of 50 m (see Figure 1), has been investigated. The channel cross-section was rectangular with a horizontal concrete bed, a width of 6 m, and a depth of flow of 0.25 m, and measurements were executed at two discharges: $0.610\,m^3/s$ and $0.305\ m^3/s$ (average velocities of about 0.4 m/s and 0.2 m/s respectively).

During these experiments the following phenomena were investigated:

a. the vertical distribution of the horizontal velocity components (main flow and helical flow);
b. the horizontal distribution of the total depth-averaged velocity; and
c. the horizontal distribution of the water surface elevation.

The experimental results have been compared with the results of a mathematical model of flow in curved open channels, developed at the Laboratory of Fluid Mechanics of the Delft University of Technology [12].

The vertical distributions of the main velocity turned out to be highly similar throughout the flow field, the distribution being well described by the logarithmic profile.
The helical velocities derived from the measured data were too inaccurate to compare them more than roughly with their theoretical distributions. The point in a cross-section where the observed depth-averaged velocity reaches its maximum lies near the inner wall in the first part of the curve and moving downstream it gradually shifts towards the outer wall. This phenomenon is attributed to the advective influence of the helical flow. As this influence is not accounted for in the present mathematical model, this model does not predict the phenomenon. The water surface configuration agreed reasonably well with the computed configuration.

FLOW OF WATER IN A CURVED OPEN CHANNEL WITH A FIXED PLANE BED

1 Introduction

Within the applied research group for sediment transport in rivers, in which Rijkswaterstaat,Directorate for water Management and Research, the Delft Hydraulics Laboratory and the Department of Civil Engineering of the Delft University of Technology collaborate, one of the research teams is concerned with water movement and sediment transport in river bends. The main purpose of this group is the development of a prediction method for the flow and the bed topography in curved alluvial rivers, which will meet the requirements of river engineering (prediction of navigability, depth of bank protection, etc.) now and in the near future. This project is incorporated in a basic research programme T.O.W. (Toegepast Onderzoek Waterstaat; Applied Research Waterstaat).

At present physical models are widely used for the above-mentioned predictions, but these models are raising a number of problems about the interpretation of the model data if great accuracy is needed. Therefore, the development of mathematical models has become attractive, even though these have their own specific limitations (schematization of the geometry and the flow, etc).

As a first step towards a mathematical model for curved alluvial rivers, a mathematical model of the flow in curved shallow channels with variable cross-section is being developed in the Laboratory of Fluid Mechanics of the Delft University of Technology. A first version of this model was tested against available experimental data from laboratory flumes, mostly with flat beds, but yielded partially negative results [12]. None of these flumes, however, had geometrical proportions corresponding to those of the Dutch natural rivers, while in addition no sufficient "prototype" data were available from these rivers.

In order to fill up these lacunae, a series of experiments was executed at the De Voorst Laboratory of the Delft Hydraulics Laboratory (where a curved channel was available, having a fixed flat bed and geometrical proportions which are representative of the Dutch river branches), and an extensive measuring programme was carried out in a bend of the River IJssel. Moreover, a second series of experiments in the Laboratory channel is planned, with a non-flat, fixed bed having a configuration of banks and troughs as in a natural bend. The results of these experiments will be published separately in a second part of this report. In this Part I the measurements in the flat bed laboratory channel are described and the results compared with results from the mathematical model.

The experiments were executed by H.J. de Vriend of the Delft University of Technology and by F.G. Koch of the Delft Hydraulics Laboratory. The present report is the result of their mutual effort.

2 Experimental set-up

During the experiments presented in this report, the flow (velocity and direction) and the elevation of the free water surface were measured in a curved fixed bed channel.

2.1 Channel geometry

The geometry of the channel is given in Figure 1. It consisted of a 38 m long straight section, followed by a 90^{o} bend with a radius of curvature of 50 m (see Figure 1). Throughout the concrete channel, the cross-section was rectangular, 6 m wide with a maximum depth of 0.30 m. The channel bed was horizontal in the straight part and had a longitudinal slope of $3 * 10^{-4}$ in the channel-axis in the curved part (see Figure 2a). The actual bed elevation is given in Figure 2b. As can be seen in this figure, the maximum deviation from the theoretical bed level was about $0.3 * 10^{-2}$ m.

This channel, originally constructed for investigations into navigation problems, was convenient for testing the mathematical model, because its most important geometric parameters (viz., the depth-width ratio and the depth-radius of curvature ratio) agreed well with those in the Dutch river branches ($d/B \leq 5 * 10^{-2}$; $d/R_c \leq 6 * 10^{-3}$); likewise, they agreed better with the basic assumptions made for the mathematical model than in most of the other channels from which experimental data are available [9]. Besides, there was a possibility for later experiments, with a fixed bed having a large-scale configuration of banks and troughs as in natural rivers. From this type of experiments very little data are available [12, 13, 14], although they are even more important for testing the mathematical model than the flat bed experiments, the channel configuration being closer to the natural one.

2.2 Flow conditions

The water inflow at the upstream end of the channel was not distributed uniformly over the channel width, as can be seen from the measured velocity distribution in cross-section A_1, Figure 18a. Perfect uniform inflow was not necessary, since the measured mean inflow distribution could be imposed at the upstream boundary of the mathematical model.

The discharge was measured and regulated by a movable Romijn weir. Two series of measurements were carried out, one with a discharge of 0.610 m^3/s (being the maximum discharge of the existing water circulation system), and the other one with a discharge of 0.305 m^3/s. In addition, the depth of flow at the upstream end of the channel was kept constant (0.25 m during both experiments, yielding average velocities of about 0.4 m/s and 0.2 m/s respectively). The depth of flow was regulated by a movable tail-gate at the downstream end of the channel. For the operation of this tail-gate, measurements of the water surface elevation were executed in the middle of cross-section A_0 and near the side walls of cross-section B_0. The discharge and the water surface elevation in these three reference points were checked regularly during the measurements, and, when necessary, the weirs (Romijn weir and tail-gate) were re-adjusted.

The most important data concerning the channel dimensions and the flow conditions are summarized in the following table, along with the Reynolds number $Re = \frac{v.h}{\nu}$ and the Froude number $Fr = \frac{v}{\sqrt{gh}}$.

discharge	depth	width			mean velocity	Reynolds number	Froude number
Q	d	B	d/B	d/radius	$\bar{v}$	Re	Fr
m^3/s	m	m	-	-	m/s	-	-
0.610	0.25	6	0.042	0.005	0.4	9.2×10^4	0.26
0.305	0.25	6	0.042	0.005	0.2	4.6×10^4	0.13

2.3 Measured data

The experimental testing of the mathematical model was concentrated on three phenomena, viz.:

- the vertical distribution of the horizontal velocity components (main flow and helical flow) (T2, for summary of the measurement numbers see Table I);
- the horizontal distribution of the total depth-averaged velocity (T3); and
- the horizontal distribution of the water surface elevation (T4).

In order to gather experimental information about these phenomena, the time-averaged magnitude and direction of the velocity vector were measured in a three-dimensional grid, using a combined current-velocity/direction meter, and the water surface elevation was measured in selected verticals of this grid, using static tubes (see Appendix A).
The measuring procedure used is described and motivated in Appendix B.

The grid points were defined by 9 cross-sections (numbered A_1 to E_0; see Figure 1a), 13 equidistant verticals in each cross-section (numbered 1 to 13, see Figure 1b) and 10 equidistant grid points per vertical (interval 0.025 m). Cross-section A_0 turned out to be unsuitable for inclusion in the grid as the flow was not yet fully established in this section situated rather close to the upstream boundary. To find out whether the tail-gate had a negligible influence on the flow in section E_0, a special series of measurements (T1) was made in this section with three different shapes of the gate (horizontal crest, straight crest inclined outward with the level at the outer wall 2 cm higher than at the inner wall, and straight crest inclined inward with the level at the inner wall 1 cm higher than at the outer wall). From these measurements it was concluded that the flow in section E_0 was not perceptibly influenced by the shape of the tail-gate (see also Section 3.1.1). Hence E_0 was included in the measuring grid.

3 Results

3.1 Experimental results

The elaboration of the measured data is described in Appendix C.

3.1.1 Influence of the shape of the tail-gate (T1)

As the tail-gate was situated in a curved section of the channel where a transverse slope of the water surface occurred, the velocity distribution along the gate could be expected to be non-uniform. To find out whether this non-uniformity influenced the flow in the most downstream cross-section of the measuring grid, E_0, a series of measurements was made in this cross-section, with three situations being examined under equal flow conditions ($Q = 0.610\ m^3/s$):

a. crest horizontal (T1-1);
b. crest inclined with the level at the outer wall 0.01 m lower than at the inner wall (T1-2); and
c. crest inclined with the level at the outer wall 0.02 m higher than at the inner wall (T1-3).

In the situations T1-2 and T1-3 the gate was made oblique by fixing a bar on it and adjusting the position of the gate until the water surface elevation in the reference points in cross-sections A_0 and B_0 was the same as in Test T1-1. In all three situations the velocities were measured at 10 points of the verticals E_03, E_07, and E_011, and the water surface elevation was measured in the verticals 1, 3, 5, 7, 9, 11 and 13 in cross-section E_0. Table V shows the results of the velocity measurements and Table VI gives the observed water surface elevations. Additionally, Figures 6-9 give a graphical respresentation.

It can be concluded from Tables V and VI and Figures 6-9 that the vertical distribution of the main velocity component and the shape of the water surface were hardly influenced by the shape of the tail-gate. The vertical distribution of the helical velocity component was too inaccurate to draw any conclusions in this respect. The only important deviation of the depth-averaged velocity was found in E_011 during test T1-2 (crest higher near the inner wall), the velocity being about 12% smaller than the overall average velocity in the section (0.383 m/s). This was no reason, however, to exclude section E_0 from the measuring grid.

3.1.2 Vertical distribution of the horizontal velocity components (T2)

The results of the 10-point velocity measurements concerning the vertical distribution of the horizontal velocity components are given in Tables VII...X and Figures 10...16.

Judging the results summarized in these tables and figures the following remarks can be made:

a. For both discharges (0.610 and 0.305 m^3/s) the vertical distributions of the normalized main velocity were similar in the various measuring stations. Only the distributions in the verticals $D_0 1$ and $D_0 13$ (i.e., the verticals the closest to the walls) tended to deviate from the other ones (figure 11): in both verticals the velocity reductions near the water surface were larger and extended over a larger part of the vertical. For the vertical near the inner wall ($D_0 13$) an explanation of this phenomenon can be found in the advective influence of the helical flow on the main velocity distribution [10, 11, 12], but from the same point of view the opposite (i.e., increase of the velocity near the water surface) should have been expected in the vertical near the outer wall, if at least the helical circulation had the same sense of rotation throughout the cross-section. On closer investigation of the flow near the outer wall, however, a counter-rotating helix turned out to occur there in the upper half of the flow (see Figures 14...16). Hence the velocity distribution in $D_0 1$ can be explained from advective effects as well.

b. There were differences between the vertical distributions of the main velocity for the two discharges. Assuming these distributions to be logarithmic (see Section 3.2.1 Eq. 1) the Chézy-factor to be derived from semi-logarithmic plots of the velocities at 0.610 m^3/s (Figure 12) was about 70 $m^{\frac{1}{2}}/s$, whereas the value derived from the plots at 0.305 m^3/s was about 50 $m^{\frac{1}{2}}/s$. In addition, the velocity reduction near the water surface was relatively larger in the former case.
The difference in the Chézy-factors cannot be explained by differences in the bed roughness, as the bed was cleaned before both measuring series. Also, as in both cases the depth of flow was approximately the same, the explanation cannot be found in a different depth of flow either.
The most plausible explanation is that the influence of the helical flow on

the main flow through advective effects was stronger at the higher flow rate. This advection caused a velocity reduction in the upper part of the flow and an increase of the velocity in the lower part. The latter can effect a steeper slope in the semi-logarithmic velocity plots, suggesting a higher value of the Chézy-factor than would occur in the corresponding straight channel flow.

c. The measurements of the helical velocity proved to be too inaccurate to draw conclusions concerning the similarity of its vertical distributions in the various verticals. If this similarity is assumed, the measured results for the cross-sections C_0, D_0 and E_0 give an indication of "the" helical velocity curve, and its possible deviation due to the inaccuracy in the measurements (Figures 13, 14, 15).

d. If there is a helical velocity in cross-section B_0, it is much smaller than in the sections further downstream (Figure 13).

e. Near the outer wall in cross-section D_0 a helical circulation in a clockwise direction occurred in the upper half of the flow, pushing the "normal" counter-clockwise rotation to the lower half (Figure 16). Dye injections near the outer wall showed this circulation to develop shortly after the beginning of the bend, to reach its maximum width (about 0.5 m) between the cross-sections C_0 and D_0 and then to decrease slowly until it had vanished between cross-sections D_1 and E_0.

3.1.3 Depth-averaged velocity field (T3)

The depth-averaged velocities resulting from the 6-point measurements (see Appendix B.2.2) throughout the channel are given in Table XI and Figure 17.

In order to compare the results for the two discharges (0.610 and 0.305 m^3/s), the depth-averaged velocities have been normalized by the mean value of the velocity in the relevant cross-section, computed from the depth-averaged values using the trapezium rule with zero velocity at the walls. The results are given in Table XII and Figure 18a.

The conclusions to be drawn from these tables and figures are:

a. The velocity distribution along the upstream boundary (cross-section A_1) is not quite uniform, and the non-uniformity has not yet damped out when the beginning of the bend is reached (cross-section B_0).

b. In the first part of the bend the velocity maximum lies near the inner wall, but gradually shifts towards the outer wall when moving further downstream.

c. When moving downstream through the bend, the region where the flow is apparently influenced by the inner wall tends to grow larger, whereas in the second half of the bend no influence of the outer wall is perceptible in the adjacent vertical (vertical 1).

d. The shifting of the velocity maximum and the increase of the inner wall influence tend to take place over a shorter longitudinal distance at the lower discharge.

3.1.4 Water surface configuration (T4)

The elevation of the water surface above a horizontal datum (viz., the bed level in the straight section of the flume) is given in Table XIII and Figure 19. The local depth of flow, obtained by subtracting the theoretical local bed level from the above-mentioned water surface elevation, is given in Table XIV and Figure 20. In Figure 20b only the curve for the average depth of flow has been drawn because of the small differences between the various verticals in a cross-section.

It can be seen from these tables and figures that:

a. At the large discharge the transverse slope of the water surface was established soon after the beginning of the bend (cross-section B_1 in Figure 19). At the smaller discharge the establishing seemed to go slower (cross-section C_1), but this is not sure because the observed configuration was disturbed by inaccuracies.

b. The water surface showed a rather strong backwater curve: $\bar{h}(E_0) - \bar{h}(B_0) = 0.0124$ m for $Q = 0.610$ m^3/s and $\bar{h}(E_0) - \bar{h}(B_0) = 0.0193$ m when $Q = 0.305$ m^3/s (see Table XIV), which implies that the average longitudinal slope of the free surface was about $1.7 * 10^{-4}$ smaller than the longitudinal slope of the bed in that part of the channel ($3.0 * 10^{-4}$) when $Q = 0.610$ m^3/s and

$2.7 * 10^{-4}$ smaller when Q = 0.305 m^3/s. Hence an additional non-uniformity of the depth-averaged velocity was introduced, although this non-uniformity was much smaller than the non-uniformity caused by the curvature (see Figure 18a).

3.2 Comparison with theoretical results

3.2.1 Vertical distribution of the horizontal velocity components

The observed vertical distributions of the main velocity have been compared with the logarithmic law:

$$v'_{main} = 1 + \frac{\sqrt{g}}{\kappa C} + \frac{\sqrt{g}}{\kappa C} \ln \frac{z}{h} \qquad (1)$$

and with the parabolic law applied by Engelund [3]:

$$v'_{main} = 1 + \frac{13}{6} \frac{\sqrt{g}}{C} \{-2 + 6 \frac{z}{h} - 3 (\frac{z}{h})^2\} \qquad (2)$$

(see Figures 10 and 11). At the higher discharge (0.610 m^3/s) the Chézy-factor chosen was C = 70 $m^{\frac{1}{2}}/s$, and at the lower discharge (0.305 m^3/s) C = 50 $m^{\frac{1}{2}}/s$ (see 3.1.2.b). In both cases Von Kármán's constant was taken 0.4.
In order to have theoretical curves that were comparable with the experimental results, the velocities found from (1) and (2) have been divided by their 10-point depth-averaged value, which was computed using the same trapezium rule as in the computation of the depth-averaged observed velocities.

The comparison of the theoretical and the experimental distributions (Figures 10 and 11) leads to the following conclusions:

a. The logarithmic distribution (1) tends to agree better with the observations than the parabolic one (2).
b. As a consequence of the advective influence of the helical circulation, the velocities observed near the water surface were smaller than predicted by the theory, whereas in the lower half of the flow they tended to be larger. These effects were the strongest near the side walls.

The observed vertical distribution of the helical velocity component has been compared with the theoretical distributions derived by De Vriend [12], Enge-

lund [3], Rozovskii [8] and Ikeda [5], using the same values for the Chezy-factor and Von Kármán's constant as in the main velocity distributions. As the individual experimental distributions were too inaccurate to draw conclusions from, the theoretical curves have only been plotted in the summarizing Figure 15, which gives an indication of "the" vertical distribution of the observed helical velocities, if this distribution is assumed to be similar in all verticals.

The conclusions to be drawn from this comparison are:

a. Ikeda's theory provides the best agreement with the measured data, whereas all other theories tend to underestimate the observed helical velocity. In Ikeda's theory the main velocity distribution is described by the logarithmic law, just as in De Vriend's and Rozovskii's, where the helical velocity distribution is solved from the transverse equation of motion in which the eddy viscosity is assumed to be constant along the vertical, as in Engelund's theory. The boundary conditions are supplied by the vanishing of the transverse shear stress both at the free surface and at the bed, and by the integral condition of a zero net transverse discharge. On theoretical grounds, however, both the inconsistency of the eddy viscosity distribution (parabolic in the main velocity computation and constant in the helical velocity computation) and the vanishing of the transverse shear stress at the bed are disputable. These objections against Ikeda's theory are not eliminated by the fair agreement with the measured data. The conclusion to be drawn from this agreement is that the parabolic eddy viscosity is not suited for modelling the present flow: the vertical distribution must be flatter in the upper part of the flow, yielding smaller values there if the vertical mean value remains the same. As the theoretical main velocity distribution is not much influenced by the distribution of the eddy viscosity in the upper part of the flow, the agreement between theory and experiment as to the main flow will not be violated if this different eddy viscosity distribution is applied. The helical velocity distribution, however, depends to a much higher extent on the eddy viscosity in the upper part of the flow, the slope of the helical velocity curve ($\Delta v'_{hel}/\Delta z$) being steeper if the eddy viscosity is smaller. Hence the flatter eddy viscosity distribution will give rise to a more intense helical flow.

b. The helical velocity distribution near the outer wall in cross-section D_0 is completely different from the theoretical curves. This could be expected, because all theories are based on the existence of one single helical circulation and they only hold far from the sidewalls. So a counter rotating circulation near the outer wall is beyond the scope of these theories.

3.2.2 Depth-averaged velocity field

The depth-averaged velocity field has been simulated numerically using the computational programme developed at the Laboratory of Fluid Mechanics of the Delft University of Technology on the basis of theoretical considerations [12]. The computational grid, consisting of a cartesian part for the straight section and a polar part for the curved section, covered the channel from cross-section A_0 (the theoretical upstream boundary) to cross-section E_0 (the theoretical downstream boundary). The longitudinal step size was 1.00 m in the channel axis, and the transverse step size was 6.00/16 = 0.375 m. At the upstream boundary a uniform velocity distribution and a zero vertical vorticity were imposed, at the downstream boundary the cross-sectional water surface elevation was taken linear, the total fall between the outer and the inner walls being equal to the observed one.

Additionally, the following values were taken for the constants: $\kappa = 0{,}4$, $C = 70\ (50)\ m^{\frac{1}{2}}/s$, $Fr = 0.226\ (0.108)$, $\underline{d}$ (average depth of flow at the downstream boundary) = 0.261 (0.272), the values for the lower discharge (0.305 m^3/s) being indicated in brackets.

The depth-averaged velocities resulting from this simulation are shown in Figure 18b. Only one set of lines has been drawn, as the computed values of the normalized depth-averaged velocity were practically the same for both discharges.

Comparing the theoretical and the experimental results (Figures 18a and b), it is seen that there is a rather poor agreement; even when the measured mean velocity distribution is imposed at the upstream boundary. Neither the shifting of the velocity maximum towards the outer wall nor the growth of the "inner wall layer" were represented by the theory. This can be explained by the advective influence of the helical circulation which is not accounted for in the mathematical model underlying the computer programme. Apparantly this effect may not be neglected, even though theoretically it is of the order of magnitude $O(h^2/R^2)$.

3.2.3 Water surface configuration

The water surface configuration computed with the aforementioned mathematical model has been compared with the measured data in Figures 19 and 20, and yields the conclusions:

a. The configuration of the water surface in transverse direction (Figure 19) is predicted fairly well at a higher discharge. At the lower discharge the agreement is poorer, especially in the first part of the flume, but it should be noted that the relative accuracy of the measured differences in the water surface is smaller than at the higher discharge.

b. The longitudinal distribution of the depth of flow (Figure 20) is better predicted at the lower discharge. The computed backwater curve, however, is strongly influenced by the value of the Chézy-factor C applied in the mathematical model. This value could be computed from the bed roughness and the flow Reynolds number, but if the bed roughness is not accurately known this yields inaccurate results. For example, if in the present case the Nikuradse bed roughness length varies between 10^{-4} m and 10^{-3} m, the computed value of C, computed by the logarithmic formula for Q = 0.610 m^3/s, varies between 79 $m^{\frac{1}{2}}/s$ and 61 $m^{\frac{1}{2}}/s$ respectively.

In straight uniform shear flow C can be estimated from the vertical distribution of the velocity and from the total energy loss along the channel, but in the present non-uniform curved flow such estimations are questionable. As was stated in Section 3.1.2, the values of C deduced from the velocity distributions are 70 $m^{\frac{1}{2}}/s$ for Q = 0.610 m^3/s and 50 $m^{\frac{1}{2}}/s$ for Q = 0.305 m^3/s.

As a consequence of the inaccurate estimation of C, comparison of the measured and the computed backwater curves does not make clear whether the "bend losses" are well predicted by the mathematical model.

4 Conclusions

1 For the present experiments the accuracy of the flow direction measurements is of predominant importance to the accuracy of the helical velocity to be derived from the measured magnitude and direction of the velocity vector (see Appendix D). Therefore, in addition to an improvement of the vertical positioning system, a careful calibration of the measuring device is wanted for this purpose.

2 The presence of the tail-gate (having a horizontal crest) in the curved section of the channel (where the water surface has a transverse slope) does not noticeably influence the flow in the last cross-section of the measuring grid, E_0, situated 7 m upstream of it.

3 The vertical distributions of the main velocity are very similar throughout the flow field, except close to the side walls in the curved part of the channel. There the main velocity is further reduced in the upper part of the flow, whereas it is higher in the lower part of the flow.

4 The vertical distribution of the main velocity is well described by the logarithmic profile, except near the water surface (where the observations show a velocity reduction, whereas the theory does not) and near the side walls in the curved part of the channel (cf. 3). These deviations can be explained qualitatively from the advective influence of the helical flow on the main flow, which is not accounted for in the logarithmic law.

5 The helical velocities derived from the measured data are too inaccurate to enable conclusions to be drawn as to the similarity of the individual vertical distributions. If all experimental results are plotted in one figure, however, most points turn out to be spread around a distinct vertical distribution curve. Only in verticals close to the outer wall do the helical velocities substantially deviate from this distribution, as a consequence of a counter rotation existing there.

6 Comparing the summarizing plots of the vertical distributions of the helical velocities with various theoretical curves derived by De Vriend [12], Rozovskii [8], Engelund [3], and Ikeda [5], Ikeda's curve turns out to

agree best with the experimental data. This suggests that the vertical distribution of the eddy viscosity is flatter than the parabolic curve applied in De Vriend's and Rozovskii's theories.

7 The observed depth-averaged velocity field shows two striking features:
   a. The point in a cross-section where the depth-averaged velocity reaches its maximum lies near the inner wall in the first part of the bend, but further downstream it gradually shifts towards the outer wall.
   b. In the bend the "inner wall region" (i.e., the region where the flow appears to be influenced by this wall) grows larger in a downstream direction.

8 The depth-averaged velocity distribution resulting from a mathematical model based on De Vriend's theory agrees poorly with the observed distribution, especially in the second part of the bend, where the shifting of the velocity maximum and the width of the inner wall region become considerable. These phenomena, to be attributed to the advective influence of the helical flow on the main flow, are not reproduced by the theory, since this influence is not accounted for in the theoretical model.

9 The mathematical model gives a rather good prediction of the transverse water surface configuration. Only in the straight part of the channel do differences between theory and experiment occur at the lower discharge.

10 The observed longitudinal distribution of the depth of flow is better predicted at the lower discharge, but no conclusions can be drawn from this, as the results strongly depend on the Chezy-factor, the value of which cannot be determined with sufficient accuracy. For the same reason, it is not clear whether the "bend losses" are well presented by the mathematical model.

Finally, it should be noted that the mathematical model used here was primarily meant to be used as a part of a mathematical model of the flow and the bed topography in curved alluvial channels. In such channels, after averaging out the ripples and dunes, the bed shows a configuration of banks and troughs that may be expected to exert a predominant influence on the flow pattern. In that case the shortcomings of the model in predicting the flow in a curved channel with a fixed flat bed may turn out to be of minor importance. To verify this

experimentally, another series of measurements will be made in the present channel, after it has been provided with a non-flat bed topography. These measurements will be discribed in Part II of this Report, to be published separately.

REFERENCES

1 BROLSMA, P.,
Temperatuurcorrectie voor micromolenmetingen,
Waterloopkundig Laboratorium, Informatie H 18, 1973

2 Combined current-velocity/direction meter,
Delft Hydraulics Laboratory, Technical description, March 1975

3 ENGELUND, F.,
Flow and bed topography in channel bends,
Proceedings of the ASCE, Journal of the Hydraulics Division, 100, HY 11, November 1974, p. 1631

4 GRIJSEN, J.G.,
Risico analyse,
Waterloopkundig Laboratorium, Speurwerkverslag S 164, Oktober 1974

5 IKEDA, S.,
On secondary flow and bed profile in alluvial curved open channel,
Proceedings of the XVIth Congress of the IAHR, 2, paper B-14, Sao Paulo, 1975

6 Investigation of the total error in measurement of flow by velocity area methods,
International Organization for Standardization, Report ISO/TC113/WG-1 (Netherlands - 16, 17, 18) 177, 178, 179, August 1971 (rev. August 1974)

7 JENKINS, G.M., and WATTS, D.G.,
Spectral Analysis and its applications,
Holden-Day series in time series analysis, San Fransisco, 1968

8 ROZOVSKII, I.L.,
Flow of water in bends of open channels,
Israel Program for Scientific Translations, Jerusalem, 1961

9 VRIEND, H.J. de,
Literatuuroverzicht bochtstroming,
Laboratorium voor Vloeistofmechanica, Afd. Weg- en Waterbouwkunde, Technische Hogeschool Delft, Rapport R 1972/1/L, 1972

REFERENCES (continuation)

10 VRIEND, H.J. de,
Theory of viscous flow in curved shallow channels,
Communications on Hydraulics, Dept. of Civil Engineering, Delft University of Technology, Report 72-1, 1973

11 VRIEND, H.J. de,
Theory of viscous flow in wide curved open channels,
Proceedings of the International Symposium on River Mechanics, Paper A17, Bangkok, Thailand, January 1973

12 VRIEND, H.J. de,
A mathematical model of steady flow in curved shallow channels,
Communications on Hydraulics, Dept. of Divil Engineering, Delft University of Technology, Report 76-1, 1976

13 YEN, C.L.,
Bed configuration and characteristics of subcritical flow in a meandering channel,
PH. D. Thesis, University of Iowa, Iowa City, Iowa (U.S.A.), 1967

14 YEN, C.L.,
Bed topography effect on Flow in a meander,
Proceedings of the ASCE, Journal of the hydraulics Division, 96, HY 1, January 1970, p. 57

appendices

Appendix A

INSTRUMENTATION

INSTRUMENTATION

1 Water surface elevation

The water surface elevation was measured with static tubes connected to a measuring pit by plastic hoses of about 15 m length (see Figure 1). Three cross-sections could be reached from one pit, which implies that three pits were needed to cover all nine cross-sections. In each pit 7 measuring glasses were mounted, sothat for each cross-section the water surface elevations in all 7 measuring points could be recorded simultaneously. The water levels in the glasses were measured by point gauges. Using a vernier fine setting an accuracy in the readings of about 10^{-4} m could be obtained. The point gauge readings were related to one datum, viz., the mean level of the horizontal bottom in the straight part of the channel.

As a consequence of the rather long connections between the static tubes and the measuring glasses, a considerable time (several hours) had to pass between the installation of the tubes and the setting of the point gauges in order to have oscillations of the water in the measuring system damped out.

2 Velocity

The magnitude and the direction of the flow were measured simultaneously by a combined current-velocity/direction meter, consisting of a miniature propeller and a vane (see Figure 3). The propeller measuring the magnitude of the velocity vector had a diameter of 0.011 m. The vane indicating the direction of the velocity vector was 0.020 m high and 0.050 m long. By means of a servo system the frame in which the propeller and the vane are mounted is turned in the flow direction. Hence the propeller measures the total velocity v_{tot}. For more technical information see [2].

The angular speed of the propeller varied linearly with the current velocity. A calibration curve (Figure 4) of the propeller gave the coefficients c_1 and c_2, necessary to convert the observed frequency (number of recorded pulses N divided by the time T) to the velocity:

$$v_{tot} = c_1 N/T + c_2 \qquad \text{(m/s)} \qquad \text{(A.1)}$$

The calibration was executed in water of a certain temperature, which implied that the coefficients c_1 and c_2 should be corrected for the actual temperature of the water in the channel. In this respect it can be remarked that only c_2 varied with the water temperature to a considerable extent, depending on the individual propeller [1]. A rough indication of this dependency is given by:

$$c_{2actual} = c_{2calibration} + 0.0234\ (\eta - \eta_0) \quad (m/s), \qquad (A.2)$$

in which:

η = the dynamic viscosity (in cp) of the water at the actual temperature
η_0 = the dynamic viscosity (in cp) of the water during the calibration

The vane turns in the flow direction and commands the frame also to turn in the flow direction by means of two position sensors and a servo system. The position of the frame is measured by means of a potentiometer. The recording equipment converts the signal to degrees. Since the flow is turbulent, the direction of the vane varies in time. The average direction over a set period is determined by using an electronic integrator.

Appendix B

MEASURING PROCEDURE

MEASURING PROCEDURE

1 Accuracy

1.1 Velocity measurements (TO-1)

In order to draw up a measuring procedure for the velocity measurements, the propeller of the flow meter was tested by putting it at a certain point in the flow and taking a long series of observations of 30 s duration each. Figure 5 shows that the observed frequencies varied slowly in time. This phenomenon could not be explained from variations in the actual velocity due to long waves in the channel, since these waves should have had an amplitude of 0.01 m in order to cause the observed velocity variations. Continuous water level registrations by an electronic "water surface follower" have shown that waves of this amplitude did not exist in the channel.

A possible explanation of the variations can be found in the pollution of the water in the circulation system, which consisted mainly of open channels. Small suspended particles gradually filled up the holes in the perforated ring around the propeller, reducing the number of perforations counted by the detector. Thus the observed frequency could decrease in time, whereas the actual frequency did not. In addition, suspended little hairs and threads accumulated around the axis of the propeller, thus increasing its rotational resistance. The further velocity measurements confirmed this theory. When checking the propeller after a series of measurements, very often particles and threads had to be removed.

The above-mentioned long test series provided the possibility of axamining the influence of the observation period on the accuracy of the velocity measurements. Taking the 30 s period as a basis, longer periods were simulated by taking the average of a number of subsequent 30 s values. Thus four test series were generated, with periods of 30, 60, 90 and 150 s, respectively. The standard deviations of each of these series were taken as an indication of the accuracy of the individual observations. Table II shows that a longer observational period yields a relatively small decrease of the standard deviation. Considerably smaller standard deviations were found if the decreasing trend in the observations was eliminated by subtracting from the data the values according to the least squares straight line (see Figure 5).

Hence, assuming the test series to be representative for all velocity measurements, the measuring procedure should eleminate the effect of a linear de-

crease of the observed values in time rather than include long observation periods.
It should be noted here that, if the linear decrease is representative and due to pollution of the measuring device, the measured velocities are always too small. The difference between the real and the measured values depends on the rate of pollution, which is difficult to estimate.

Another way to obtain an impression of the accuracy of the velocity measurements in relation to the observation period is to consider the standard deviation of the instantaneous signal from the measuring device as a function of time. During a protracted observation (say 300 s) the signal was sampled every 0.1 s and the standard deviation was computed continuously. This standard deviation turned out to have reached its final value after about 30 s, from which it was concluded that an observation period of 30 s would be sufficient to eliminate the turbulent fluctuations.

1.2 Flow direction measurements (TO-2)

The current flow direction meter was developed for measurements in large-scale models of tidal regions, where deviation angles upto 180° occur. In that case, an accuracy of some degrees is sufficient. In the present experiments, however, the angles of deviation to be measured were some degrees, so much higher demands had to be made on the accuracy.

There were three important sources of errors in the measuring system:
a. the backlash in the mechanical steering system;
b. the backlash in the transmission between the steering and recording system and the vertical shaft the vane was mounted on; and
c. the calibration procedure of the instrument.

a Errors due to backlash in the steering system

The instantaneous error caused by this backlash can be 5°, but as the deviation angle of the vane is subject to turbulent fluctuations and the steering system has to follow these, the effect of the backlash will be eliminated by averaging over a sufficiently long period. To get an impression of the necessary length of this period, a number of test measurements was executed, recording the average value of the deviation angle (computed continuously on

the basis of 0.1 s samples of the signal from the apparatus) as a function of time. Table III shows that after 1 to 2 minutes the average has reached its final value.

b Errors due to backlash in the transmission

The shaft on which the propeller and the vane were mounted (see Figure 3) had to be moved vertically when positioning the propeller and the vane at a certain level. For this purpose a key was sunk into a keyway in the shaft, which was gripped by friction only. The backlash in this transmission varied between 1^{o} and 5^{o}, depending on the individual apparatus. The position of the shaft within this variation changed every time the shaft was given a vertical displacement, which was done by hand. The steering system was not able to surmount the friction between the key and the keyway, so the above errors were not eliminated by averaging, like the errors due to backlash in the steering system. If, after positioning the instrument in some grid point, the shaft was given a small, always positive or always negative, deviation angle, the key would always be placed at the same end of its backlash. It has been tried to eliminate the transmission error this way, but according to the results (see Section 3.1.2) this was not always successful.

The apparatus used in the present experiments turned out to have a rather small transmission error: about 1.5^{o}. This was assessed by positioning the instrument in a grid point and measuring the deviation angle of the flow using a fairly long observation period (say 2 minutes) sothat turbulent fluctuations were eliminated. The measurements were repeated several times, alternately after giving the shaft a positive and a negative initial rotation, the observation starting some time after the positioning in order to let the vane turn to the real flow direction. By doing this, two groups of results were to be discerned according to whether the initial angle was positive or negative. Between these groups there was a significant difference in the measured angles of about 1.5^{o}.

c Errors due to the calibration procedure

The calibration of the direction meter was done only statically, i.e., outside the flow. The apparatus was put on a sheet of paper with parallel lines on it, so placed that these lines were perpendicular to the front of the apparatus. The frame around the vane containing the sensors of the steering system was then put into the direction of the lines and the recorder output was set at

0°. Subsequently, the frame was turned over 180° and the potentiometer in the electronic recording system was calibrated in such a way that the recorder gave an output of 180°.
As the positioning was done visually, it always had to be executed by the same person. A multiple repetition of the procedure showed that an absolute positioning accuracy of about 0.5° could then be reached. But as the direction meter was not calibrated dynamically, either in a towing tank or in a real flow, the accuracy of the representation of the instantaneous flow angle by the vane remains uncertain.

The helical velocity component was strongly influenced by errors in the flow deviation angle, as shown in Appendix D. On the other hand, the main velocity component and the depth-averaged velocity were hardly influenced by these errors. When computing the helical velocity component from the measured data, the depth-averaged direction of the flow was eliminated. Hence the systematic error in the zero reference angle played no part in this component.
The most severe errors are those mentioned under b, due to the backlash in the transmission system. Calibration errors in the scale factor of the recorder (180° output = 180° measured) were hardly felt because of the smallness of the measured angles.

2 Measuring procedure

2.1 Positioning of the flow meter and the static tubes

The positioning of the flow meter in the three-dimensional grid was done in three steps:

a. Fixing the cross-section: In the side walls of the channel metal pins marked the points of intersection of these walls and the cross-sections A_0 to E_0. The two pins in a cross-section fitted into two holes in the axis of a movable bridge across the channel that could thus be place perpendicular to the channel axis.

b. Fixing the vertical: In the measuring domain the above-mentioned bridge had a wide groove around the axis, through which the shaft of the flow meter could be moved up and down.

The position of the verticals was marked on the bridge by stripes and the shaft on the flow meter could be positioned vertically in these verticals by using a spirit level fixed to the apparatus. In order to have the same reference angle throughout the cross-section, the front of the apparatus was put parallel to the bridge axis.

c. Fixing the grid point: The fixed bed was taken as a reference for the position of the grid points in a vertical. The distance between the lowest point of the measuring device and the axis of the propeller was about 0.025 m, and by placing the lowest point of the instrument just above the bed, the velocities and deviation angles at 0.025 m above the bed could be measured. In that position the distance from a fixed point of the shaft to the case of the instrument (which could not be moved vertically) was measured by a ruler. All higher grid points were referred to this lowest point by moving up the shaft over the required distance. Thus an accuracy in the vertical positioning of about 0.005 m could be attained, which was thought to be sufficient.

The static tubes were mounted on a transportable bar across the channel, in such a way that the tubes were positioned in the seven verticals of the measuring grid for the water surface elevation if the bar was placed in a cross-section. For practical reasons, the bar was not placed in the cross-section, but about 0.5 m downstream of it. The water surface elevations measured there diferred very little from those in the cross-section itself: the difference caused by a longitudinal slope of 10^{-4} is $5 * 10^{-5}$, which is withing the accuracy of the measurements. Thus the velocities and the water surface elevations could be measured simultaneously without any delay due to the long time of adjustment of the water level measuring system.

2.2 Velocity measurements (T2, T3)

For the part of the measurements concerning the vertical distributions of the velocity components a limited number of verticals was selected, viz., in the centre-line of the cross-sections B_0, C_0, D_0 and E_0 and the verticals 1, 4, 10 and 13 of cross-section D_0.
In all grid points of these verticals, i.e., at 0.025, 0.050, 0.075,..., 0.200, 0.225 m from the bed and as close to the water surface as possible (T2), the

magnitude and the direction of the velocity vector were measured twice during 60 s. The measurements started in the lower grid point and successively moved up to the surface point, where two subsequent observations were taken. Then successively lower points were revisited until the point near the bed was reached. Subsequently the apparatus was removed from the water, the propeller was cleaned and the measurements restarted in the next vertical. In this way the linear decrease in time of the velocity measurements mentioned in Section B.1.1 was eliminated if the time interval between two subsequent measurements was eliminated if the time interval between two subsequent measurements was constant throughout the vertical. For the part of the experiments concerning the depth-averaged velocity field, only 6 grid points were selected in a vertical line, viz., at 0.025, 0.050, 0.100, 0.150, and 0.200 m from the bed and as close as possible to the water surface (T3). In these points the magnitude and the direction of the velocity vector were measured, following the same procedure as in the above-mentioned vertical distribution measurements. To find out how the reduction to 6 points in a vertical worked out on the depth-averaged value of the velocity, 10-point observations in two verticals, $E_0 3$ and $E_0 7$, have been averaged and compared with the averaged values obtained when selecting 6 points out of these 10. Table IV shows that the error introduced by the selection is less than 1%. This table also shows that there is no difference between a selection with two adjacent points near the bed and a selection with two adjacent points near the surface.

2.3 Surface elevation measurements (T4)

During both series of velocity measurements (T2 and T3), the water surface elevation was measured every few hours, during the vertical distribution series (T2) in the relevant verticals, during the depth-averaged flow series (T3) in the verticals 1, 3, 5, 7, 9, 11 and 13 of each cross-section. If more than one value per vertical was measured, the observed elevations were averaged in order to find "the" elevation in the relevant vertical.

Appendix C

ELABORATION OF MEASURED DATA

ELABORATION OF MEASURED DATA

The data obtained from the velocity measurements, viz., the number of pulses given by the velocity meter during the observation period and the average value of the flow deviation angle, had to be elaborated to velocity components and depth-averaged velocities. This was done by the following steps:

a. Averaging of both number of pulses and deviation angles that were found in each grid point, yielding the average number of pulses N and the average deviation angle.

b. Computation of the total velocity in each grid point from:

$$v_{tot} = c_1 N/T + c_{2_0} + .0234(\eta-\eta_0) \qquad \text{(m/s)} \qquad \text{(C.1)}$$

in which c_1 = the slope of the calibration curve ($= \frac{dv}{df}$ in m)

c_{2_0} = the value of v at which the calibration curve intersects the v-axis (m/s)

η = the dynamic viscosity of the water at the actual temperature (cp)

η_0 = the dynamic viscosity of the water at the rating temperature (cp)

T = the observational period (in s)

The constants of the calibration curve in Figure 5 are: $c_1 = 0.000921$ m and $c_{2_0} = 0.021$ m/s.

c. Computation of the tangential and the radial velocity components v_t and v_r from:

$$v_t = v_{tot} \cos\phi \qquad \text{(C.2)}$$

$$v_r = v_{tot} \cos\phi \qquad \text{(C.3)}$$

ϕ being positive when the flow is directed outward.

d. Computation of the depth-averaged tangential and radial velocity components $\bar{v}_t$ and $\bar{v}_r$ using the trapezium rule:

$$\bar{f} = \frac{1}{h} \sum_{i=1}^{n} (z_i - z_{i-1})(f_i + f_{i-1})/2 + (h - z_n)f_n \qquad \text{(C.4)}$$

in which f = the function to be averaged
h = the local depth of flow
z = the elevation of the grid points above the bed
i = the number of the grid point (i=1 is the point near the bed)
n = number of grid points in the vertical

The quantities z_0 and f_0 were taken equal to zero, as the velocity may be expected to vanish at the bed.

e. Computation of the magnitude $\bar{v}_{tot}$ and the direction α of the depth-averaged velocity vector from:

$$\bar{v}_{tot} = (\bar{v}_t^2 + \bar{v}_r^2)^{\frac{1}{2}} \tag{C.5}$$

$$\alpha = \frac{\pi}{180} \text{ atan } (\bar{v}_r/\bar{v}_t) \tag{C.6}$$

f. Computation of the main velocity component (defined as the component in the direction of the depth-averaged velocity vector) and the helical velocity component (defined as the component perpendicular to the direction of the depth-averaged velocity vector) from:

$$v_{main} = v_{tot} \cos (\phi - \alpha) \tag{C.7}$$

$$V_{hel} = v_{tot} \sin (\phi - \alpha) \tag{C.8}$$

g. Normalization of the above-mentioned velocity components in order to make their distributions in different verticals comparable. In a first approximation, the theoretical velocity components are proportional to $\bar{v}_{tot}$ (main component) and $\bar{v}_{tot}$ h/R (helical component) [12]. Hence the normalized velocity components are defined by:

$$v'_{main} = v_{main}/\bar{v}_{tot} \tag{C.9}$$

$$v'_{helical} = v_{helical} \text{ R/h } \bar{v}_{tot}), \tag{C.10}$$

in which R is the local radial coordinate.

This normalization was necessary in order to compare the vertical distributions of the velocity components in different verticals.

The elaborations were executed on a computer, using a simple FORTRAN-programme written for this occasion.

Appendix D

INFLUENCE OF ERRORS IN THE MEASURED DATA

INFLUENCE OF ERRORS IN THE MEASURED DATA

In order to obtain an impression of how errors in the measured data work out on the results of the elaboration procedure described in Appendix C, an analysis of the errors in these results was made by numerical simulation (using the Monte Carlo method).

1 Summary of measured quantities

The quantities measured during or in relation to the present experiments can be divided into four groups:

a. General constants (invariant throughout the experiments or large parts of them):
   - 1/2 the two coefficients determining the velocity rating line (see Appendix A and Figure 4): c_1 and c_2,
   - 3 the rating coefficient of the flow angle: c_3,
   - 4 the water temperature during the calibration of the velocity meter: $temp_c$,
   - 5 the coefficient of proportionality c_4 in the correction term of c_2 in Equation (A.2), accounting for the deviation from $temp_c$ of the water temperature $temp_m$ during the measurements. This coefficient was not determined for the present instrument, but was estimated on the basis of earlier experiments [1].

b. Vertical constants (invariant in each vertical, but variable from vertical to vertical):
   - 1 the radial coordinate R,
   - 2 the local depth of flow: h,
   - 3 the reference angle of the direction meter: ϕ_0'.

c. Point constants (invariant during an observation in a point, but variable from point to point):
   - 1 the vertical distance to the bed: z_i ($i = 0,1,\ldots,np$; $z_0 = 0$),
   - 2 the duration of the observation: T,
     As T was chosen constant (30 s; 60 s) for all measuring points in each part of the experiments, it can be considered as a general constant.
   - 3 the water temperature $temp_m$. This quantity did not perceptibly change

during the measurements in a vertical, hence it can be considered as a vertical constant.

d. Instantaneously variable quantities (randomly varying during an observation in a point):
   1 the instantaneous velocity,
   2 the instantaneous flow angle.
   As only the time-average of these quantities is considered, they have been replaced by:
   1' the number of pulses n to be counted by the velocity meter during the observation period,
   2' the time-average of the flow deviation angle ϕ'.

2 Summary of errors taken into account

Measuring or estimating the quantities above introduced systematic and random errors and, additionally, errors were introduced by using observations of limited duration to determine the time-averaged velocities and flow angles. As accounting for all possible errors would become too laborious, the errors that may be expected to be of minor importance to the results of the elaboration have been neglected.
Dividing the errors into the same four groups as the quantities to be measured (Section D.1) yields:

a. General systematic errors (invariant throughout the experiments or large parts of it):
   All of these errors are very small with respect to the true values of the relevant quantities, except the error in c_4 [1]. As the temperature of the water during the measurements did not deviate more than 3°C from the calibration temperature, however, the correction term for c_2 in Equation (A.2) is small with respect to c_2 and even smaller with respect to the measured values of v_{tot}. Hence all general systematic errors have been neglected.

b. Errors that are systematic in a vertical (i.e., invariant in a vertical, but randomly varying from vertical to vertical):

1 The error in the measured local depth of flow H *), which is assumed to have had a normal distribution with expectation 0 and standard deviation σ_H.

2 The error in the measured reference angle of the direction meter ϕ_0', as far as it was due to errors in the determination of the zero reference angle and the positioning of the instrument in a vertical (see Appendix B). This error was assumed to be normally distributed, too, with expectation 0 and standard deviation $\sigma_{\phi_0'}$.

3 The error in the positioning of the instrument in the lowest point of the vertical (i=1). As all higher points were referred to the lowest point in the relevant vertical, the error in the determination of the vertical distance Z_1, of this point to the bed must be considered as being systematic for that vertical. This error, dZ_1, has been assumed to be normally distributed with expectation 0.0015 and standard deviation σ_{dZ_1}.

4 The error in the velocity measurements due to the gradual pollution of the propeller. Assuming the decrease in the measured velocity caused by this pollution to be linear in time and the measurements to be made with constant time intervals, this error has been considered as an error in the coefficient C_1 of the velocity rating line, being constant in a vertical. It is assumed to have had a limited normal distribution with expectation μ_{dC_1} and standard deviation σ_{dC_1}, limited to $dC_1 \leqq 0$.

All other errors of this type (for instance in R) have been neglected.

c. Errors that are systematic in a point (i.e., invariant during an observation in a point, but randomly varying from point to point):

1 The error dZ in $Z_i - Z_1$ ($i = 2,3,\ldots,np$), which has been assumed to be normally distributed with expectation 0 and standard deviation σ_{dZ} (constant throughout a vertical).

2 The error in the flow deviation angle ϕ' due to the backlash in the keyway (see Appendix B). As this error could only be introduced when displacing the vane to another measuring point, it was constant during an observation. This was expected to be one of the most severe errors in the present experiments, so special attention had to be paid to its

* The measured values are indicated by capital letters

probability distribution.

A normal distribution would not have been adequate here, since the error is limited due to the limited backlash and if there was a maximum in the probability density function, it would occur at both ends of the backlash rather than somewhere in between. Therefore, in the numerical simulation two different probability density functions have been applied, once with a uniform distribution between the limits $d\phi'_k = \pm a$ and once with a distribution consisting of two Dirac-functions in $d\phi'_k = -a$ and $+a$, respectively.

3/4 The errors in N and ϕ' due to the limited duration of the observation period. These errors have been treated in combination with the effect of the errors in the velocity and direction measurements mentioned in category d.

All other errors of this type have been neglected.

d. Instantaneously variable errors:

The instantaneously variable errors introduced when measuring the instantaneously variable velocities and flow deviation angles are not important to the time-averaged values of these quantities if the observation period is sufficiently long. The average over the observation period of a random variable with zero expectation will then approach this expectation. However, a separate empirical investigation of this type of error is hardly possible, unless another measuring device of far better quality at this point is available. Through lack of such a device, the approximate time-averaged quantities N (or rather N/T) and ϕ' were investigated (see Appendix B), only yielding information regarding the combined effect of errors due to the imperfection of the measuring system (instantaneously variable) and errors due to the limited duration of the observation period. These combined errors must be considered as being of type c and replacing the errors mentioned under c 3/4.

Further investigations into these errors (to be reported in Part II) have shown that the variances of the random variables N (or rather N/T) and ϕ' vary along a vertical, having a maximum at the bed and decreasing when moving upward until, near the surface, a small increase again occurred. Moreover, the covariance between the errors in N and ϕ' turned out to be negligible.

In addition to the errors introduced by measuring or estimating the input data of the elaboration procedure, this procedure introduces an important error itself when using the trapezium rule, Equation (C.4), for averaging the tangential and radial velocity components over the depth of flow.
This error depends on the number of points taken in a vertical. An indication of its magnitude is obtained by averaging the basic logarithmic curve, Equation (1), having the exact average value 1, using Equation (C.4). Both in the 10-point case and in the 6-point case the values found from Equation (C.4) are about 3% too small. The small difference between these two cases can be explained from their similarity near the bed, the most critical region of the vertical in this respect.

3 Numerical simulation

3.1 General outline of the method

The simulation method can be summarized as follows [4]:

a. the probability density functions of the random input data of the simulated process being given, a set of values of these data was chosen using a random procedure
b. the operations on the input data constituting the process were carried out and the results to be studied have been stored
c. the above routine (a-b) has been repeated many times, yielding a large number of values for each of the output quantities to be considered
d. considering the values obtained for a certain output quantity as samples of a random variable, they have been analyzed to yield the probability density function of this quantity

Thus the probability density function of each of the results of the process could be determined. For further details of the method and its evaluation, see Reference [4].

In terms of the present problem this implies that:

- a large number of sets of "measured data" has been generated using a random procedure
- the elaboration procedure described in Appendix C when applied to each set of measured data, yields a large number of values of the quantities to be studied, i.e., $\bar{v}_{tot}$, α, v'_{main_i} and v'_{hel_i} $(i = 1,2,\ldots,np)$.

- from these values the probability density function of each of these quantities is derived

3.2 Quantification of input data

The values attributed to the various quantities playing a part in the error analysis have been summarized in Tables XV, XVI, XVII and XVIII.
The values in Table XVIII of the expectations of N and ϕ' between the given points were estimated by linear interpolation, with the standard deviations being assumed to be constant about each point.
All random quantities were assumed to be uncorrelated.

3.3 Results

A general conclusion to be drawn from the results of the numerical simulation is that all resultant random errors are normally distributed, even though the errors in the input data, especially $d\phi'_k$, are not. This implies that each of the results is fully characterized by its mean and its standard deviation.

In Table XIX the results of the numerical error analysis are given together with the expected values of the quantities without errors.
In addition, the results for v'_{main} and v'_{hel} are given in Figure 21.

From these results it is concluded that the most severe errors occur in α and v_{tot} and that the influence of $d\phi'_k$ is predominant in v'_{hel}, but not in α.
An additional run with $\phi'_0 = 0$ yielded a much smaller standard deviation in α, whereas v'_{hel} was not influenced at all. From this it can be concluded that ϕ'_0 is the main source of errors in α rather than $d\phi'_k$.

tables

measurement serial number	discharge m^3/s	description	measurement	location
T0		test series	a series of velocity and direction measurements to establish the measuring procedure (see Appendix B)	not relevant
T0-1	0.610	flow velocity measurement		
T0-2	0.610	flow direction measurement		
T1		influence shape of tail gate	flow velocity and direction	cross-section E_o verticals 3,7,11 All 10 grid points [4]
T1-1	0.610	horizontal crest		
T1-2	0.610	crest 0.01 m lower at the outer wall	water surface elevation (see Chapter 3.1.1)	cross-section E_o verticals 1,3,5,7,9,11,13
T1-3	0.610	crest 0.02 m higher at the outer wall		
T2		vertical distribution of velocity (main flow and helical flow)	60 sec. average flow velocity and direction measured twice in each grid point	cross-sections B_o,C_o,E_o vertical 7 cross-section D_o verticals 1,4,7,10,13 all 10 grid points [4]
T2-1	0.610			
T2-2	0.305			
T2-3	0.610	distribution near the outer wall		cross-section D_o verticals ½,2 [3] all 10 grid points [4]
T3		horizontal distribution of total depth-averaged main velocity	30 sec. average flow velocity and direction measured twice in each grid point	all cross-sections [1] all verticals [2] grid points: 2.5,5,10,15,20,25
T3-1	0.610			
T3-2	0.305			
T4		horizontal distribution of water surface elevation	water surface elevation was measured twice during measurement T2 and twice during T3	all cross-sections [1] verticals 1,3,5,7,9,11,13
T4-1	0.610			
T4-2	0.305			

1) i.e. cross-sections A_1, A_2, B_o, B_1, C_o, C_1, D_o, D_1, E_o } see Figure 1

2) i.e. verticals 1 to 13 incl.

3) Vertical ½ is an extra vertical between the outer wall and vertical 1

4) i.e. grid points 2.5, 5, 7.5, 10, 12.5, 15, 17.5, 20, 22.5, and 25 (the Figures indicate the height in cm above the channel bed in a vertical)

Table I Summary of measurements

measurement sequence number	observed (30 sec)	2-point average (60 sec)	3-point average (90 sec)	5-point average (150 sec)
1	11935	11901		
2	11867	11824	11861	
3	11780	11851	11856	11917
4	11922	12002	11928	11924
5	12082	12026	11991	11953
6	11969	11990	12020	11958
7	12010	11908	11928	11949
8	11806	11843	11898	11885
9	11879	11819	11815	11850
10	11759	11777	11811	11778
11	11794	11723	11735	11856
12	11651	11924	11881	11792
13	12197	11878	11802	11821
14	11559	11732	11887	11853
15	11904	11929	11805	11884
16	11953	11880	11888	11802
17	11807	11797	11849	11835
18	11787	11756	11773	11761
19	11724	11629	11682	11722
20	11534	11646	11672	11666
21	11758	11643	11607	11646
22	11528	11608	11658	11630
23	11687	11664	11619	11669
24	11641	11686	11686	11658
25	11731	11716	11691	11733
26	11701	11804	11779	11744
27	11906	11824	11783	11757
28	11741	11723	11784	11711
29	11705	11603	11649	11700
30	11500	11574	11618	11612
31	11648	11557	11538	11507
32	11466	11341	11443	11528
33	11216	11513	11497	11521
34	11809	11637	11496	11507
35	11464	11522	11618	11518
36	11580	11550	11521	11609
37	11520	11597	11591	11570
38	11674	11644	11603	11598
39	11674	11644	11603	
40	11604			
average	11735	11734	11734	11734
stand. dev.	189	153	145	137
after subtraction of the least squares line:				
average	0	-5	-1	-1
stand. dev.	143	92	79	62

Table II Number of counted holes during propeller test (TO-1)

duration of observation in sec	deviation angle in degrees									
	observations close to the bed						observations at 0.20 m above the bed			
	1	2	3	4	5	6	7	8	9	10[1)]
10	-2.6	-0.5	-0.9	-1.2	-0.3	-0.5	+4.3	+4.0	+3.5	+3.8
20	-1.9	-0.8	-1.3	-0.8	+1.1	-1.0	+4.1	+4.0	+4.2	+4.0
30	-1.7	-0.8	-1.4	-0.6	-0.9	-1.1	+4.1	+3.9	+4.1	+3.9
40	-1.4	-1.1	-1.2	-0.7	-0.9	-0.7	+4.1	+4.0	+4.1	+3.9
50	-1.4	-1.1	-1.1	-0.7	-0.8	-0.4	+4.0	+4.0	+3.9	+3.8
60	-1.4	-1.1	-1.2	-0.7	-0.9	-0.3	+4.0	+4.0	+3.9	+3.7
70	-1.3	-1.2	-1.3	-0.7	-0.8	-0.4	+4.0		+4.0	
80	-1.2	-1.2		-0.8	-0.8	-0.6				
90	-1.2	-1.2		-0.7	-1.0	-0.6				
100	-1.3				-1.1	-0.7				
110	-1.3				-1.2	-0.8				
120	-1.2				-1.2	-0.8				
130	-1.2									

[1)] The numbers 1 to 10 indicate different observations

Table III Deviation angle versus observation period (TO-2)

grid point (m above the bed)	total velocity in m/s					
	vertical $E_0 3$			vertical $E_0 7$		
	10-point average	6-point average	6-point average	10-point average	6-point average	6-point average
0.025	0.342	0.342	0.342	0.352	0.352	0.352
0.050	0.376	0.376		0.386	0.386	
0.075	0.394		0.394	0.405		0.405
0.100	0.404	0.404		0.420	0.420	
0.125	0.417		0.417	0.430		0.430
0.150	0.431	0.431		0.440	0.440	
0.175	0.435		0.435	0.444		0.444
0.200	0.436	0.436		0.451	0.451	
0.225	0.433		0.433	0.448		0.448
0.250	0.407	0.407	0.407	0.422	0.422	0.422
average	0.388	0.386	0.386	0.399	0.398	0.398

Table IV Averaging routines for the depth-averaged velocity

vertical	grid point level (m)	velocities in m/s											
		measurement TI-1				measurement TI-2				measurement TI-3			
		v_t	v_r	v_{main}	v_{hel}	v_t	v_r	v_{main}	v_{hel}	v_t	v_r	v_{main}	v_{hel}
$E_0 3$	0.025	0.342	-0.012	0.342	-0.012	0.332	-0.029	0.333	-0.019	0.341	-0.030	0.341	-0.025
	0.050	0.375	-0.020	0.375	-0.020	0.369	-0.026	0.369	-0.014	0.363	-0.013	0.363	-0.008
	0.075	0.393	-0.007	0.393	-0.007	0.375	-0.039	0.376	-0.028	0.386	-0.013	0.386	-0.008
	0.100	0.404	0.000	0.404	-0.000	0.392	-0.027	0.393	-0.015	0.399	-0.014	0.399	-0.009
	0.125	0.417	-0.007	0.417	-0.008	0.400	-0.021	0.400	-0.008	0.412	-0.014	0.412	-0.009
	0.150	0.431	0.000	0.431	-0.000	0.408	-0.021	0.408	-0.008	0.423	0.007	0.422	0.013
	0.175	0.435	-0.008	0.435	-0.008	0.411	-0.007	0.411	0.006	0.423	0.000	0.423	0.006
	0.200	0.436	0.000	0.436	-0.000	0.412	0.007	0.412	0.020	0.426	0.000	0.426	0.006
	0.225	0.432	0.023	0.432	0.022	0.417	0.015	0.416	0.028	0.425	0.015	0.425	0.020
	0.250	0.406	0.035	0.406	0.035	0.402	0.021	0.401	0.034	0.406	0.007	0.405	0.012
	average	0.388	0.000	0.388		0.373	-0.012	0.374		0.382	-0.005	0,382	
$E_0 7$	0.025	0.351	-0.025	0.351	-0.019	0.341	-0.018	0.341	-0.022	0.334	-0.018	0.334	-0.016
	0.050	0.385	-0.027	0.385	-0.021	0.376	-0.013	0.375	-0.018	0.375	-0.007	0.375	-0.005
	0.075	0.405	-0.014	0.405	-0.008	0.398	-0.007	0.398	-0.012	0.389	-0.014	0.389	-0.012
	0.100	0.419	-0.015	0.420	-0.008	0.409	-0.007	0.409	-0.012	0.397	-0.007	0.397	-0.005
	0.125	0.430	-0.008	0.430	-0.001	0.422	0.000	0.422	-0.005	0.407	-0.021	0.407	-0.019
	0.150	0.440	0.000	0.440	0.007	0.429	0.000	0.429	-0.005	0.412	0.007	0.412	0.009
	0.175	0.444	0.008	0.444	0.014	0.439	0.008	0.439	0.002	0.423	0.000	0.423	0.002
	0.200	0.450	0.024	0.450	0.030	0.439	0.023	0.439	0.018	0.425	0.000	0.425	0.002
	0.225	0.448	0.000	0.448	0.007	0.442	0.031	0.442	0.026	0.419	0.022	0.419	0.024
	0.250	0.422	-0.007	0.422	-0.001	0.428	0.030	0.428	0.025	0.399	0.014	0.399	0.016
	average	0.399	-0.006	0.399		0.393	0.005	0.393		0.379	-0.002	0.379	
$E_0 11$	0.025	0.344	-0.018	0.344	-0.017	0.304	-0.016	0.304	-0.025	0.342	-0.030	0.342	-0.029
	0.050	0.382	-0.020	0.382	-0.019	0.329	-0.011	0.328	-0.021	0.376	-0.026	0.376	-0.025
	0.075	0.396	-0.014	0.396	-0.013	0.350	-0.006	0.349	-0.017	0.392	-0.021	0.392	-0.020
	0.100	0.404	-0.021	0.404	-0.020	0.355	0.012	0.355	0.002	0.405	-0.007	0.405	-0.006
	0.125	0.420	-0.007	0.420	-0.006	0.359	0.006	0.359	-0.005	0.409	0.000	0.409	0.001
	0.150	0.424	0.000	0.424	0.001	0.360	0.013	0.360	0.002	0.415	0.000	0.415	0.001
	0.175	0.426	0.015	0.426	0.016	0.368	0.000	0.368	-0.011	0.421	0.007	0.421	0.008
	0.200	0.422	0.015	0.422	0.016	0.363	0.032	0.364	0.021	0.414	0.022	0.414	0.023
	0.225	0.413	0.002	0.413	0.023	0.357	0.037	0.358	0.027	0.411	0.022	0.411	0.022
	0.250	0.388	0.020	0.388	0.021	0.342	0.036	0.343	0.026	0.391	0.020	0.391	0.021
	average	0.383	-0.001	0.383		0.332	0.010	0.332		0.379	-0.001	0.379	

Table V Velocities in cross-section E_0

measurement serial number	verticals in cross-section E_0						
	1	3	5	7	9	11	13
	water surface elevations in m above the bed						
T1-1	0.2615	0.2612	0.2609	0.2607	0.2602	0.2602	0.2599
T1-2	0.2662	0.2660	0.2658	0.2655	0.2651	0.2648	0.2646
T1-3	0.2681	0.2677	0.2674	0.2671	0.2669	0.2666	0.2663

Table VI Water surface elevations in cross-section E_0

measurement serial number	grid point level	main velocities							
		cross-section B_0		cross-section C_0		cross-section D_0		cross-section E_0	
		v_{main}	v'_{main}	v_{main}	v'_{main}	v_{main}	v'_{main}	v_{main}	v'_{main}
	m	m/s	-	m/s	-	m/s	-	m/s	-
T2-1 (Q = 0.610 m^3/s)	0.025	0.381	0.911	0.375	0.904	0.372	0.919	0.349	0.881
	0.050	0.419	1.002	0.410	0.988	0.395	0.975	0.382	0.965
	0.075	0.429	1.026	0.429	1.034	0.418	1.032	0.402	1.015
	0.100	0.439	1.050	0.440	1.060	0.425	1.049	0.416	1.051
	0.125	0.454	1.086	0.448	1.080	0.442	1.091	0.429	1.083
	0.150	0.458	1.096	0.457	1.101	0.441	1.089	0.433	1.093
	0.175	0.466	1.115	0.462	1.113	0.447	1.104	0.441	1.114
	0.200	0.464	1.110	0.465	1.120	0.456	1.126	0.447	1.129
	0.225	0.452	1.081	0.450	1.084	0.442	1.091	0.439	1.109
	(0.250)[1]	0.436	1.043	0.435	1.048	0.425	1.049	0.429	1.083
T2-2 (Q = 0.305 m^3/s)	0.025	0.162	0.857	0.154	0.846	0.156	0.862	0.149	0.856
	0.050	0.180	0.952	0.169	0.929	0.170	0.939	0.166	0.954
	0.075	0.193	1.021	0.179	0.984	0.182	1.006	0.170	0.983
	0.100	0.197	1.042	0.185	1.016	0.186	1.028	0.181	1.040
	0.125	0.207	1.095	0.195	1.071	0.194	1.072	0.186	1.069
	0.150	0.208	1.101	0.199	1.093	0.195	1.077	0.186	1.069
	0.175	0.210	1.111	0.203	1.115	0.203	1.122	0.191	1.098
	0.200	0.215	1.138	0.210	1.154	0.203	1.122	0.197	1.132
	0.225	0.217	1.148	0.211	1.159	0.206	1.138	0.198	1.138
	(0.250)[1]	0.213	1.127	0.209	1.148	0.203	1.122	0.197	1.132

[1] not exactly 0.250 m, but as close to the free water surface as possible

Table VII Vertical distribution of the main velocity in the channel axis

measurement serial number	grid point level	main velocities									
		vertical 1		vertical 4		vertical 7		vertical 10		vertical 13	
		v_{main}	v'_{main}	v_{main}	v'_{main}	v_{main}	v'_{main}	v_{main}	v'_{main}	v_{main}	v'_{main}
	m	m/s	-	m/s	-	m/s	-	m/s	-	m/s	-
T2-1	0.025	0.352	0.900	0.351	0.898	0.372	0.919	0.356	0.890	0.315	0.940
(Q = 0.610	0.050	0.390	0.997	0.389	0.995	0.395	0.975	0.397	0.992	0.344	1.027
m^3/s)	0.075	0.410	1.049	0.401	1.026	0.418	1.032	0.411	1.027	0.361	1.078
	0.100	0.428	1.095	0.412	1.054	0.425	1.049	0.422	1.055	0.366	1.093
	0.125	0.436	1.115	0.423	1.082	0.442	1.091	0.437	1.092	0.374	1.116
	0.150	0.434	1.110	0.430	1.100	0.441	1.089	0.438	1.095	0.371	1.107
	0.175	0.426	1.090	0.437	1.118	0.447	1.104	0.444	1.110	0.369	1.101
	0.200	0.423	1.082	0.439	1.123	0.456	1.126	0.446	1.115	0.359	1.072
	0.225	0.412	1.054	0.429	1.097	0.442	1.091	0.436	1.090	0.338	1.009
	(0.250)[1)]	0.395	1.010	0.404	1.033	0.425	1.049	0.424	1.060	0.328	0.979
T2-2	0.025	0.155	0.875	0.153	0.860	0.156	0.862	0.154	0.865	0.127	0.920
(Q = 0,305	0.050	0.168	0.949	0.165	0.927	0.170	0.939	0.169	0.949	0.136	0.986
m^3/s)	0.075	0.185	1.045	0.182	1.022	0.182	1.006	0.178	1.000	0.147	1.065
	0.100	0.191	1.079	0.183	1.028	0.186	1.028	0.184	1.034	0.153	1.109
	0.125	0.195	1.102	0.187	1.051	0.194	1.072	0.192	1.079	0.153	1.109
	0.150	0.197	1.113	0.195	1.096	0.195	1.077	0.194	1.090	0.154	1.116
	0.175	0.196	1.107	0.198	1.112	0.203	1.122	0.197	1.107	0.151	1.094
	0.200	0.194	1.096	0.202	1.135	0.203	1.122	0.200	1.124	0.151	1.094
	0.225	0.191	1.079	0.204	1.146	0.206	1.138	0.202	1.135	0.142	1.029
	(0.250)[1)]	0.186	1.051	0.202	1.135	0.203	1.122	0.197	1.107	0.135	0.978

[1)] not exactly 0.250 m, but as close to the free water surface as possible

Table VIII Vertical distribution of the main velocity in cross-section D_o

measurement serial number	grid point level	helical velocities							
		cross-section B_0		cross-section C_0		cross-section D_0		cross-section E_0	
		v_{hel}	v'_{hel}	v_{hel}	v'_{hel}	v_{hel}	v'_{hel}	v_{hel}	v'_{hel}
	m	m/s	-	m/s	-	m/s	-	m/s	-
T2-1	0.025	-0.003	-1.59	-0.024	-11.31	-0.013	- 6.29	-0.022	-10.60
(Q = 0.610	0.050	-0.002	-0.94	-0.006	- 2.78	-0.013	- 6.35	-0.018	- 8.41
m^3/s)	0.075	-0.001	-0.54	-0.011	- 5.06	-0.007	- 3.21	-0.014	- 6.87
	0.100	-0.001	-0.55	-0.005	- 2.61	-0.010	- 4.70	-0.013	- 6.06
	0.125	-0.003	-1.90	-0.006	- 2.66	0.003	1.43	-0.005	- 2.34
	0.150	0.010	5.67	0.005	2.25	0.009	4.41	0.006	2.67
	0.175	0.005	3.04	0.013	6.14	0.008	4.08	0.013	6.01
	0.200	-0.004	-2.39	0.007	3.45	0.005	2.25	0.016	7.57
	0.225	-0.001	-0.57	0.012	5.60	0.011	5.53	0.020	9.63
	(0.250)[1]	-0.001	-0.55	0.020	9.41	0.008	3.88	0.019	9.04
T2-2	0.025	-0.004	-4.25	-0.007	- 7.57	-0.012	-12.35	-0.011	-12.20
(Q = 0.305	0.050	-0.001	-0.72	-0.008	- 8.29	-0.006	- 5.88	-0.010	-11.04
m^3/s)	0.075	-0.001	-0.77	-0.003	- 3.41	-0.008	- 7.98	-0.004	- 4.47
	0.100	-0.002	-1.99	-0.006	- 6.14	-0.002	- 2.30	-0.002	- 2.32
	0.125	-0.000	-0.41	0.001	0.76	-0.001	- 0.96	-0.001	- 0.60
	0.150	0.003	2.96	0.001	0.77	0.003	3.37	-0.001	- 0.96
	0.175	-0.000	-0.42	0.004	4.00	0.003	3.51	0.004	4.88
	0.200	0.000	0.45	0.006	6.36	0.005	5.02	0.007	8.04
	0.225	0.002	2.64	0.007	7.13	0.007	7.77	0.007	8.10
	(0.250)[1]	0.003	3.46	0.007	7.09	0.008	8.77	0.008	9.18

[1] not exactly 0.250 m, but as close to the free water surface as possible

Table IX Vertical distribution of the helical velocity in the channel axis

measurement serial number	grid point level	helical velocities									
		vertical 1		vertical 4		vertical 7		vertical 10		vertical 13	
		v_{hel}	v'_{hel}	v_{hel}	v'_{hel}	v_{hel}	v'_{hel}	v_{hel}	v'_{hel}	v_{hel}	v'_{hel}
	m	m/s	-	m/s	-	m/s	-	m/s	-	m/s	-
T2-1	0.025	-0.013	-8.52	-0.023	-11.78	-0.013	- 6.29	-0.020	- 9.35	-0.015	- 8.67
(Q = 0.610	0.050	-0.002	-1.21	-0.020	-10.20	-0.013	- 6.35	-0.016	- 7.45	-0.010	- 5.66
m^3/s)	0.075	0.001	0.65	-0.010	- 5.40	-0.007	- 3.21	-0.014	- 6.68	-0.009	- 5.22
	0.100	0.007	4.69	-0.006	- 3.29	-0.010	- 4.70	-0.005	- 2.30	-0.005	- 2.72
	0.125	0.010	6.83	0.004	2.02	0.003	1.43	-0.002	- 0.93	-0.001	- 0.52
	0.150	-0.003	-1.85	0.002	0.88	0.009	4.41	0.001	0.52	0.003	1.71
	0.175	0.011	7.18	0.011	5.68	0.008	4.08	0.012	5.70	0.006	3.56
	0.200	0.002	1.66	0.014	7.30	0.005	2.25	0.012	5.73	0.009	5.26
	0.225	-0.005	-3.69	0.017	8.70	0.011	5.53	0.019	9.22	0.010	5.98
	(0.250)[1]	-0.009	-6.32	0.015	7.82	0.008	3.88	0.015	7.21	0.014	7.78
T2-2	0.025	-0.006	-5.73	-0.010	-11.42	-0.012	-12.35	-0.008	- 8.25	-0.008	-10.80
(Q = 0.305	0.050	-0.001	-1.43	-0.008	- 8.48	-0.006	- 5.88	-0.009	-10.00	-0.007	- 8.53
m^3/s)	0.075	0.000	0.06	-0.006	- 6.15	-0.008	- 7.98	-0.005	- 5.85	-0.004	- 4.61
	0.100	-0.002	-1.97	-0.003	- 3.35	-0.002	- 2.30	-0.004	- 3.99	-0.002	- 2.43
	0.125	0.003	2.82	0.001	1.63	-0.001	- 0.96	0.001	0.91	0.001	0.96
	0.150	0.003	3.19	0.002	2.46	0.003	3.37	0.002	2.39	0.001	1.31
	0.175	0.003	3.54	0.006	6.33	0.003	3.51	0.005	5.38	0.003	4.30
	0.200	-0.001	-0.62	0.006	6.86	0.005	5.02	0.004	4.35	0.004	5.65
	0.225	0.000	0.06	0.007	7.69	0.007	7.77	0.005	5.14	0.005	6.60
	(0.250)[1]	0.000	0.06	0.004	4.50	0.008	8.77	0.008	8.74	0.005	6.84

[1] not exactly 0.250 m, but as close to the free water surface as possible

Table X Vertical distribution of the helical velocity in cross-section D_o

measurement serial number	vertical	cross-section								
		A_1	A_2	B_0	B_1	C_0	C_1	D_0	D_1	E_0
T3-1	1	0.375	0.361	0.360	0.353	0.382	0.386	0.398	0.400	0.397
(Q = 0.610	2	0.371	0.370	0.383	0.371	0.372	0.376	0.401	0.401	0.399
m^3/s)	3	0.370	0.376	0.384	0.371	0.383	0.375	0.393	0.389	0.386
	4	0.373	0.387	0.388	0.379	0.384	0.381	0.399	0.396	0.389
	5	0.387	0.385	0.393	0.385	0.394	0.384	0.405	0.399	0.390
	6	0.390	0.394	0.389	0.392	0.391	0.392	0.402	0.402	0.390
	7	0.391	0.399	0.405	0.401	0.401	0.384	0.412	0.388	0.396
	8	0.411	0.414	0.414	0.406	0.405	0.400	0.409	0.409	0.390
	9	0.405	0.409	0.404	0.407	0.402	0.398	0.406	0.402	0.394
	10	0.381	0.390	0.394	0.409	0.404	0.397	0.407	0.401	0.387
	11	0.366	0.380	0.391	0.400	0.397	0.392	0.397	0.394	0.381
	12	0.376	0.380	0.390	0.395	0.390	0.372	0.378	0.368	0.351
	13	0.349	0.362	0.369	0.371	0.347	0.329	0.333	0.323	0.310
	average	0.362	0.366	0.371	0.369	0.370	0.364	0.376	0.371	0.363
T3-2	1	0.180	0.177	0.167	0.165	0.173	0.181	0.181	0.176	0.176
(Q = 0.305	2	0.174	0.178	0.175	0.172	0.179	0.179	0.181	0.179	0.179
m^3/s)	3	0.180	0.180	0.183	0.178	0.181	0.177	0.176	0.170	0.170
	4	0.188	0.186	0.186	0.180	0.182	0.180	0.179	0.174	0.172
	5	0.191	0.187	0.188	0.184	0.184	0.180	0.176	0.176	0.176
	6	0.188	0.188	0.190	0.188	0.187	0.186	0.179	0.179	0.176
	7	0.193	0.192	0.190	0.192	0.190	0.184	0.182	0.182	0.173
	8	0.202	0.202	0.197	0.197	0.190	0.186	0.183	0.178	0.174
	9	0.202	0.195	0.196	0.193	0.189	0.185	0.179	0.177	0.175
	10	0.185	0.186	0.189	0.192	0.186	0.183	0.178	0.174	0.172
	11	0.190	0.183	0.188	0.194	0.185	0.178	0.174	0.169	0.168
	12	0.179	0.179	0.186	0.187	0.179	0.168	0.162	0.156	0.153
	13	0.167	0.167	0.175	0.172	0.155	0.148	0.138	0.133	0.131
	average	0.177	0.176	0.176	0.175	0.173	0.170	0.166	0.163	0.161

Table XI Depth-averaged total velocity $\bar{v}_{tot}$ in m/s

measurement serial number	vertical	cross-section								
		A_1	A_2	B_0	B_1	C_0	C_1	D_0	D_1	E_0
T3-1	1	1.036	0.985	0.971	0.957	1.033	1.062	1.057	1.077	1.093
(Q = 0.610	2	1.025	1.010	1.033	1.006	1.006	1.034	1.065	1.080	1.099
m^3/s)	3	1.023	1.026	1.036	1.006	1.036	1.032	1.044	1.047	1.063
	4	1.031	1.056	1.047	1.027	1.038	1.048	1.060	1.066	1.071
	5	1.070	1.051	1.060	1.044	1.065	1.056	1.076	1.074	1.074
	6	1.078	1.075	1.049	1.062	1.057	1.078	1.068	1.083	1.074
	7	1.081	1.089	1.093	1.087	1.084	1.056	1.095	1.045	1.090
	8	1.136	1.130	1.117	1.100	1.095	1.100	1.087	1.101	1.074
	9	1.119	1.116	1.090	1.103	1.087	1.095	1.079	1.083	1.085
	10	1.053	1.064	1.063	1.109	1.093	1.092	1.081	0.180	1.066
	11	1.012	1.037	1.055	1.084	1.074	1.078	1.055	1.061	1.049
	12	1.039	1.037	1.052	1.071	1.055	1.023	1.004	0.991	0.967
	13	0.965	0.988	0.995	1.006	0.938	0.905	0.885	0.870	0.854
T3-2	1	1.016	1.006	0.946	0.941	1.001	1.068	1.090	1.081	1.095
(Q = 0.305	2	0.983	1.011	0.992	0.981	1.035	1.056	1.090	1.100	1.113
m^3/s)	3	1.016	1.023	1.037	1.015	1.047	1.044	1.060	1.044	1.057
	4	1.062	1.057	1.054	1.027	1.053	1.062	1.078	1.063	1.070
	5	1.079	1.063	1.065	1.049	1.064	1.062	1.060	1.081	1.095
	6	1.062	1.068	1.077	1.072	1.082	1.097	1.078	1.100	1.095
	7	1.090	1.091	1.077	1.095	1.099	1.085	1.096	1.118	1.076
	8	1.141	1.148	1.116	1.124	1.099	1.097	1.102	1.093	1.082
	9	1.141	1.108	1.111	1.101	1.093	1.091	1.078	1.087	1.088
	10	1.045	1.057	1.071	1.095	1.076	1.080	1.072	1.069	1.070
	11	1.073	1.040	1.065	1.106	1.070	1.050	1.047	1.038	1.045
	12	1.011	1.017	1.054	1.067	1.035	0.991	0.975	0.958	0.952
	13	0.943	0.949	0.992	0.981	0.896	0.873	0.831	0.817	0.815

Table XII Normalized depth-averaged velocity $\bar{v}_{tot} * \frac{A}{Q}$

measurement serial number	vertical	cross-section								
		A_1	A_2	B_0	B_1	C_0	C_1	D_0	D_1	E_0
T4-1	1	0.2516	0.2499	0.2485	0.2477	0.2460	0.2446	0.2424	0.2412	0.2401
(Q = 0.610	3	0.2516	0.2498	0.2486	0.2476	0.2457	0.2442	0.2420	0.2408	0.2398
m^3/s)	5	0.2517	0.2499	0.2485	0.2472	0.2454	0.2440	0.2418	0.2406	0.2395
	7	0.2517	0.2501	0.2482	0.2468	0.2448	0.2439	0.2415	0.2402	0.2391
	9	0.2518	0.2502	0.2482	0.2465	0.2449	0.2434	0.2414	0.2400	0.2387
	11	0.2519	0.2502	0.2479	0.2462	0.2444	0.2430	0.2407	0.2395	0.2380
	13	0.2520	0.2501	0.2475	0.2458	0.2438	0.2438	0.2404	0.2393	0.2379
	average	0.2517	0.2500	0.2482	0.2468	0.2450	0.2437	0.2415	0.2402	0.2390
T4-2	1	0.2533	0.2531	0.2527	0.2526	0.2514	0.2514	0.2512	0.2507	0.2508
(Q = 0.305	3	0.2537	0.2531	0.2528	0.2527	0.2517	0.2515	0.2510	0.2505	0.2505
m^3/s)	5	0.2536	0.2532	0.2527	0.2526	0.2515	0.2513	0.2508	0.2506	0.2506
	7	0.2537	0.2532	0.2528	0.2525	0.2516	0.2512	0.2506	0.2504	0.2503
	9	0.2536	0.2535	0.2530	0.2526	0.2514	0.2512	0.2510	0.2507	0.2508
	11	0.2539	0.2536	0.2529	0.2525	0.2514	0.2511	0.2505	0.2504	0.2503
	13	0.2540	0.2534	0.2528	0.2524	0.2513	0.2509	0.2505	0.2500	0.2500
	average	0.2537	0.2533	0.2528	0.2526	0.2515	0.2512	0.2508	0.2505	0.2505

Table XIII Water surface elevation in m

measurement serial number	vertical	cross-section								
		A_1	A_2	B_0	B_1	C_0	C_1	D_0	D_1	E_0
T4-1	1	0.2516	0.2499	0.2485	0.2513	0.2532	0.2554	0.2568	0.2592	0.2617
(Q = 0.610	3	0.2516	0.2498	0.2486	0.2512	0.2529	0.2550	0.2564	0.2588	0.2614
m^3/s)	5	0.2517	0.2499	0.2485	0.2508	0.2526	0.2548	0.2562	0.2586	0.2611
	7	0.2517	0.2501	0.2482	0.2504	0.2520	0.2547	0.2559	0.2582	0.2607
	9	0.2518	0.2502	0.2482	0.2501	0.2521	0.2542	0.2558	0.2580	0.2603
	11	0.2519	0.2502	0.2479	0.2498	0.2516	0.2538	0.2551	0.2575	0.2596
	13	0.2520	0.2501	0.2475	0.2494	0.2510	0.2536	0.2548	0.2573	0.2595
	average	0.2517	0.2500	0.2482	0.2504	0.2522	0.2545	0.2559	0.2582	0.2606
T4-2	1	0.2533	0.2531	0.2527	0.2562	0.2586	0.2622	0.2656	0.2687	0.2724
(Q = 0.305	3	0.2537	0.2531	0.2582	0.2563	0.2589	0.2623	0.2654	0.2685	0.2723
m^3/s)	5	0.2536	0.2532	0.2527	0.2562	0.2587	0.2621	0.2652	0.2686	0.2722
	7	0.2537	0.2532	0.2528	0.2561	0.2586	0.2620	0.2650	0.2684	0.2719
	9	0.2536	0.2535	0.2530	0.2562	0.2586	0.2620	0.2654	0.2688	0.2724
	11	0.2539	0.2536	0.2529	0.2561	0.2586	0.2619	0.2649	0.2684	0.2719
	13	0.2540	0.2534	0.2528	0.2560	0.2585	0.2617	0.2649	0.2681	0.2718
	average	0.2537	0.2533	0.2528	0.2562	0.2587	0.2620	0.2652	0.2685	0.2721

Table XIV Depth of flow ($z_s - z_b$) in m

c_1	c_2	c_3	c_4	η_c	η_m	T	R
m	m/s	-	m/s/cp	cp	cp	sec	m
9.23×10^{-4}	3.64×10^{-2}	1.0	0.0234	1.08	1.08	60	50.0

Table XV Quantities which are invariant throughout the simulation

H		Φ'_0		dZ_1		dC_1	
m		degrees		m		m	
exp	σ_H	exp	$\sigma_{\phi'_0}$	exp	σ_{dZ_1}	exp	σ_{dC_1}
0.260	0.001	0	0.5	0.0015	0.001	-10^{-5}	10^{-5}

Table XVI Quantities varying randomly from vertical to vertical

dZ		$d\Phi'_k$(I)	$d\Phi'_k$(II)
m		degrees	degrees
exp	σ_{dZ}	uniform distribution: for $-a \leq d\Phi'_k \leq a$: $f = \frac{1}{2a}$ else: $f = 0$	"double δ"-distribution: for $d\Phi'_k = \pm a$: $f = \frac{1}{2}\,\delta(\pm a)$ else $f = 0$
0	0.001	a = 0.75	a = 0.75

Table XVII z-independent quantities varying from point to point

grid point number i	grid point level (z) m	N		Φ' degrees	
		exp.	st.dev.	exp.	st. dev.
(0)	0	0	300	− 4.0	0.30
1	0.025	20780	300	− 2.9	0.28
2	0.050	22860	300	− 2.0	0.27
3	0.075	24160	300	− 1.3	0.25
4	0.100	24940	260	− 0.6	0.24
5	0.125	25460	220	− 0.1	0.23
6	0.150	25980	170	+ 0.5	0.22
7	0.175	26500	130	+ 1.1	0.20
8	0.200	27020	130	+ 1.5	0.19
9	0.225	27540	130	+ 1.9	0.18
10	0.250	27800	130	+ 2.4	0.17
(11)	0.260	27800	130	+ 2.6	0.16

Table XVIII z-dependent quantities varying from observation to observation

quantity	I: $d\Phi'_k$ uniform		II: $d\Phi'_k$ double δ		no errors
	mean	st.dev.	mean	st.dev.	expect.
$\bar{v}_{tot}$ (m/s)	0.4095	0.0043	0.4095	0.0043	0.4087
α (degr.)	0.1879	0.5190	0.1905	0.5412	0.1491
v'_{main_1}	0.882	0.0081	0.882	0.0082	0.878
v'_{main_2}	0.959	0.0081	0.958	0.0081	0.958
v'_{main_3}	1.009	0.0075	1.009	0.0075	1.008
v'_{main_4}	1.037	0.0065	1.037	0.0065	1.038
v'_{main_5}	1.058	0.0059	1.058	0.0059	1.058
v'_{main_6}	1.077	0.0044	1.077	0.0044	1.078
v'_{main_7}	1.097	0.0038	1.097	0.0039	1.097
v'_{main_8}	1.116	0.0037	1.116	0.0037	1.117
v'_{main_9}	1.135	0.0039	1.135	0.0039	1.136
$v'_{main_{10}}$	1.144	0.0040	1.144	0.0040	1.146
v'_{hel_1}	-8.942	1.002	-8.987	1.567	-8.999
v'_{hel_2}	-6.870	1.104	-6.842	1.782	-6.915
v'_{hel_3}	-4.876	1.110	-4.845	1.776	-4.904
v'_{hel_4}	-2.618	1.104	-2.630	1.769	-2.610
v'_{hel_5}	-0.837	1.145	-0.860	1.801	-0.884
v'_{hel_6}	+1.159	1.170	+1.048	1.852	+1.269
v'_{hel_7}	+3.459	1.187	+3.426	1.849	+3.502
v'_{hel_8}	+5.035	1.192	+5.089	1.921	+5.065
v'_{hel_9}	+6.714	1.191	+6.788	1.996	+6.681
$v'_{hel_{10}}$	+8.631	1.188	+8.667	1.940	+8.662

Table XIX Results of the numerical error analysis

figures

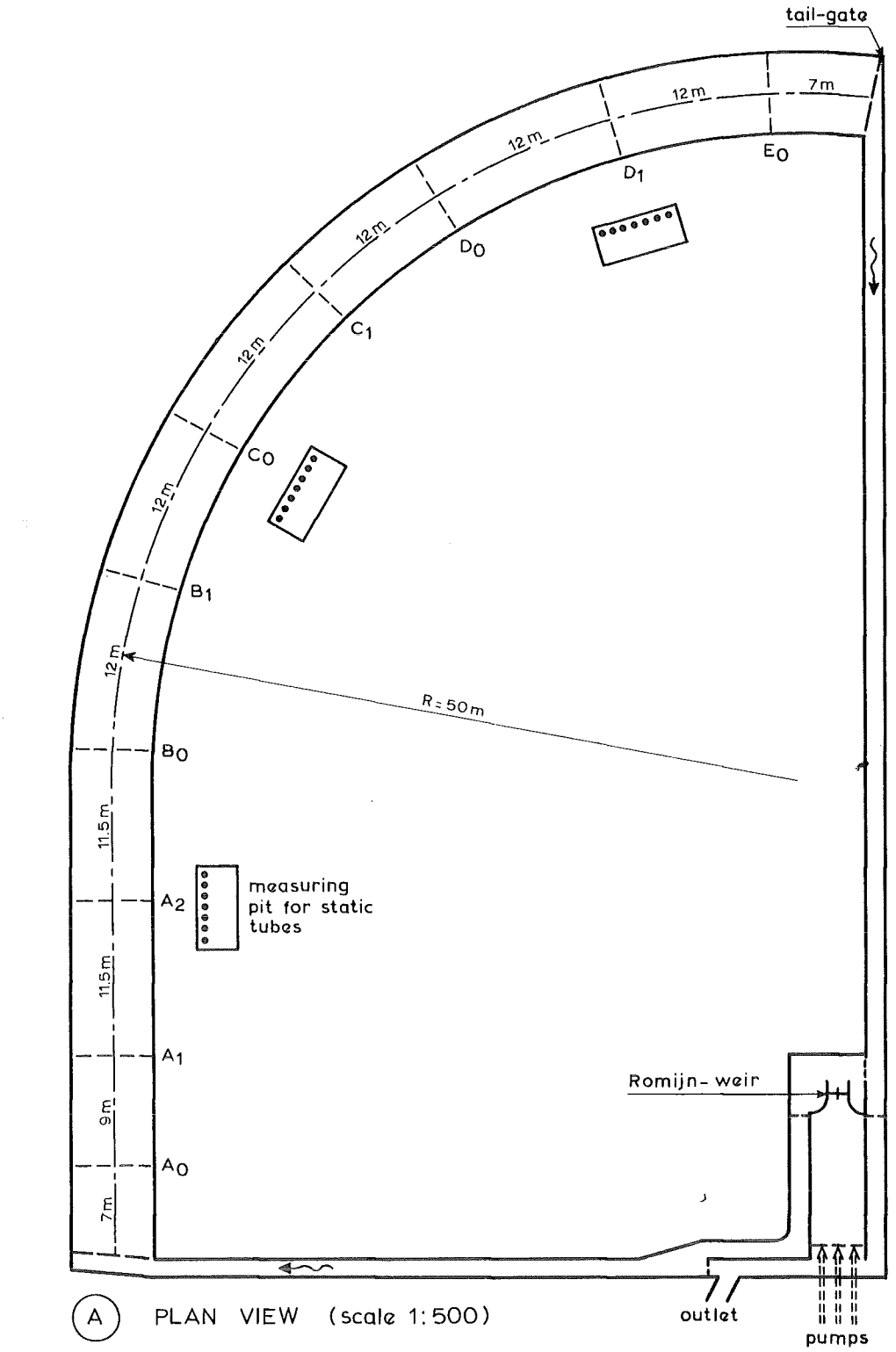

A PLAN VIEW (scale 1:500)

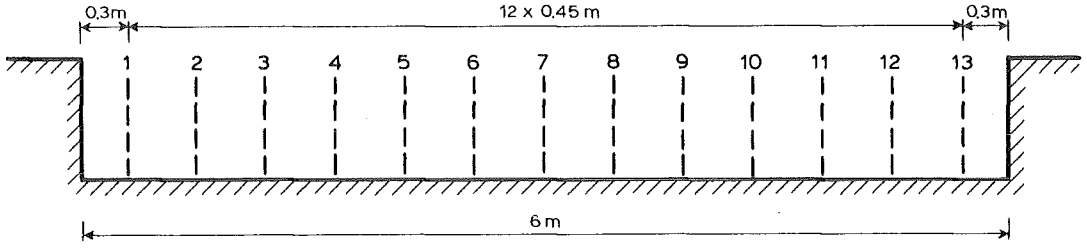

B CROSS-SECTION (scale 1:50)

CHANNEL GEOMETRY

DELFT HYDRAULICS LABORATORY/DELFT UNIVERSITY OF TECHNOLOGY | R657/M1415 | FIG. 1

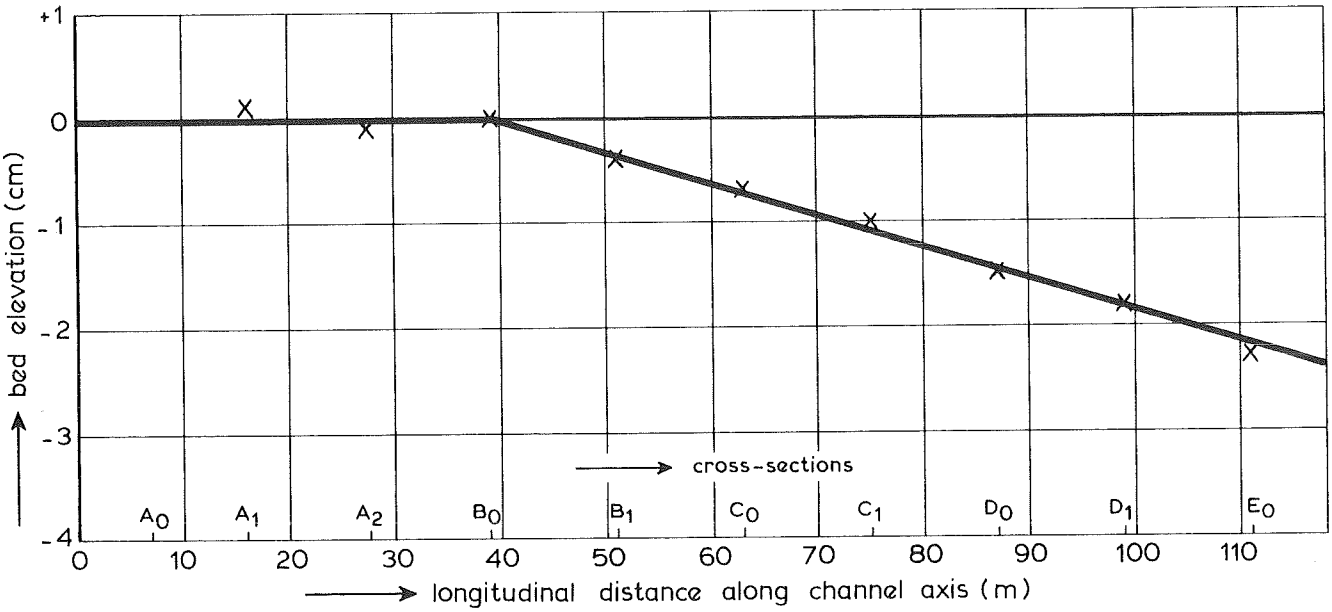

X average measured channel bed elevation (average of 13 measurements in each cross-section)

(A) BED ELEVATION ALONG CHANNEL AXIS

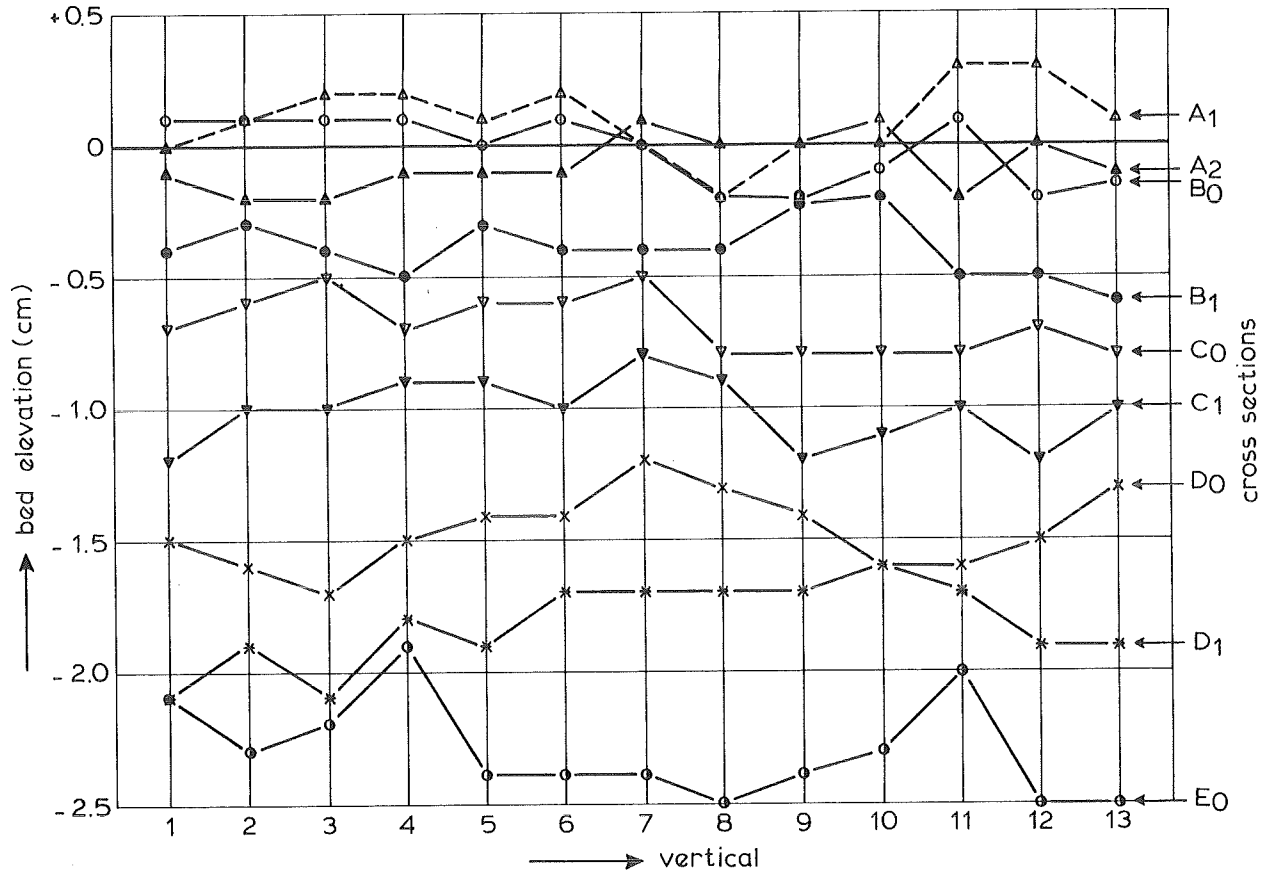

(B) BED ELEVATION OF CROSS-SECTIONS

BED ELEVATION		
DELFT HYDRAULICS LABORATORY/DELFT UNIVERSITY OF TECHNOLOGY	R657/M1415	FIG. 2

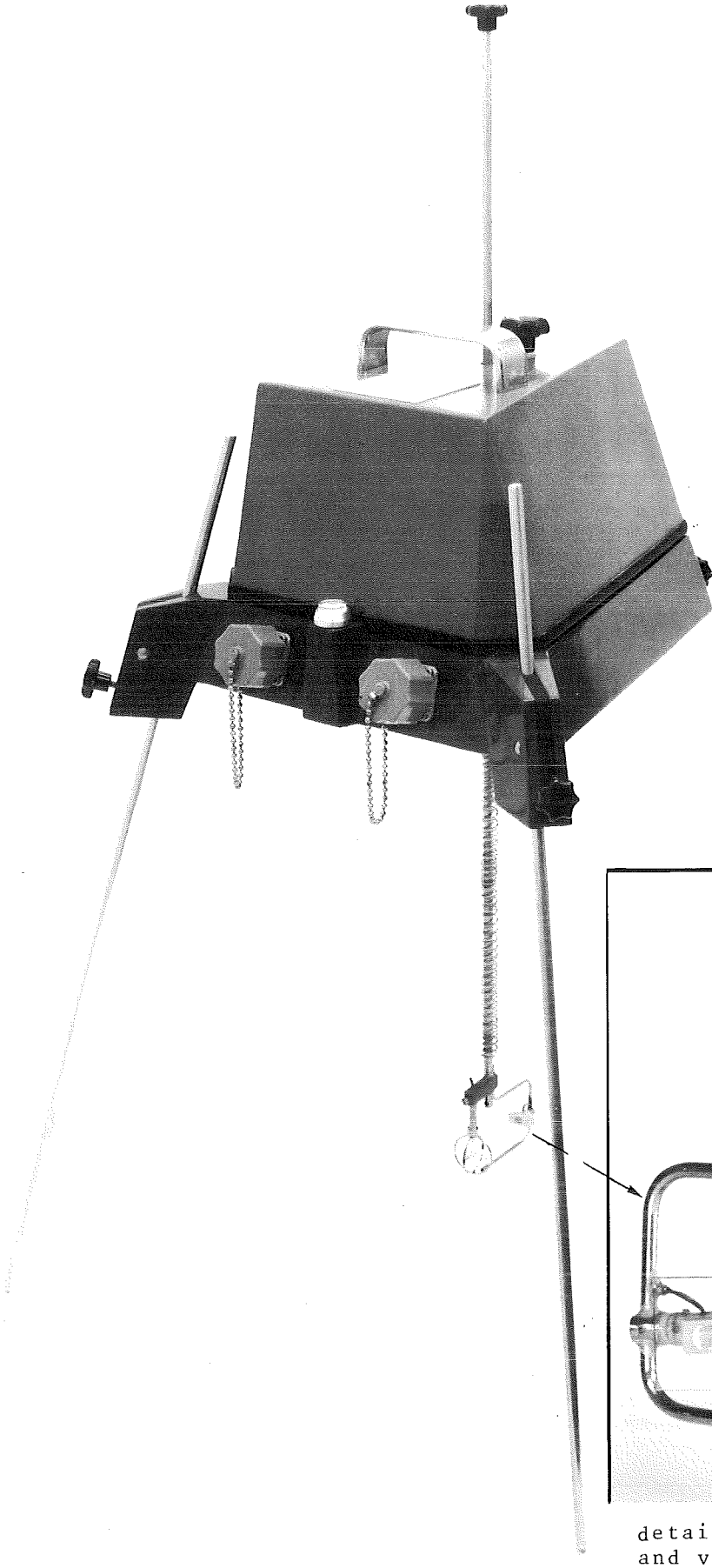

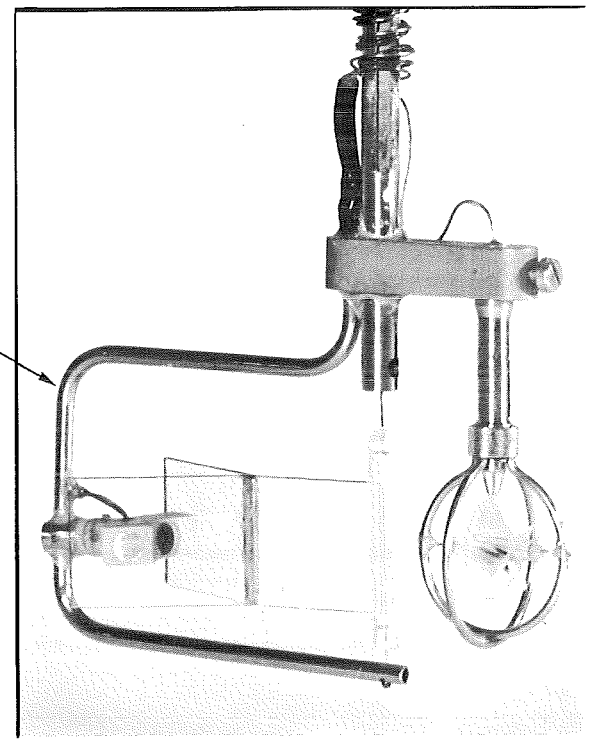

detail of the direction vane
and velocity meter

Combined current-velocity/direction
meter

FIG. 3

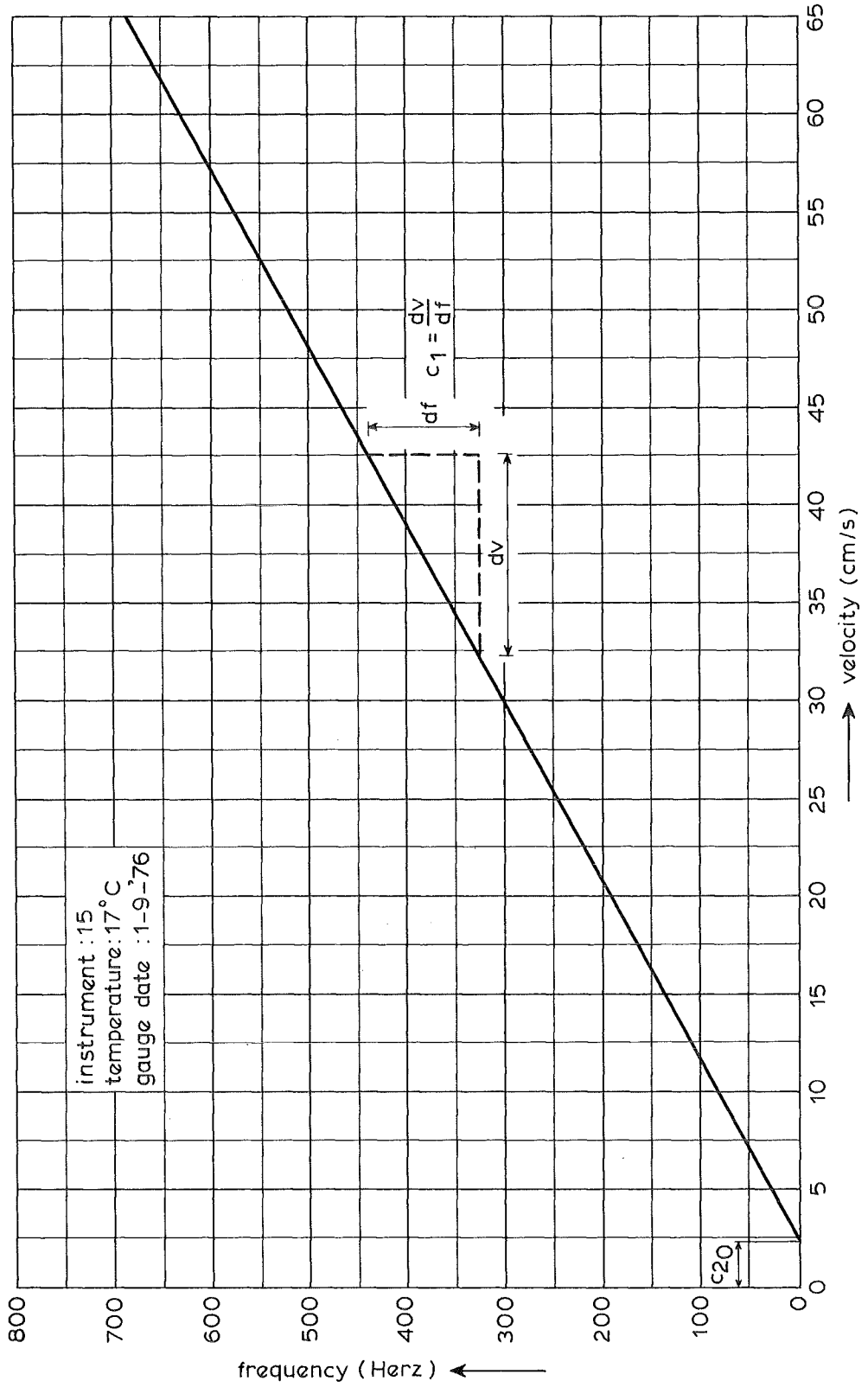

CALIBRATION CURVE VELOCITY METER

DELFT HYDRAULICS LABORATORY/ DELFT UNIVERSITY OF TECHNOLOGY | R657/M1415 | FIG. 4

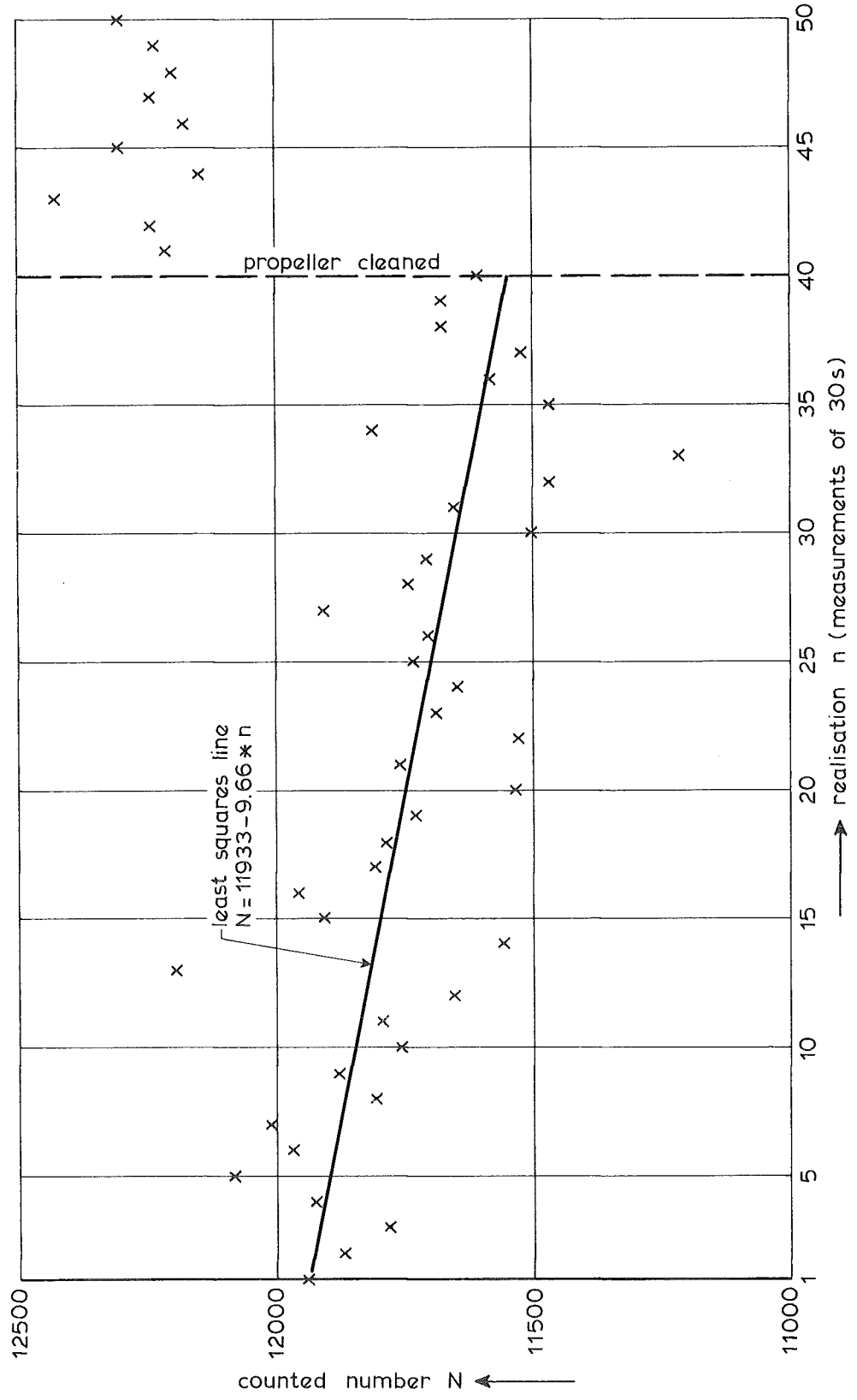

TEST SERIES OF VELOCITY MEASUREMENTS	T 0 – 1	
DELFT HYDRAULICS LABORATORY/DELFT UNIVERSITY OF TECHNOLOGY	R657/M1415	FIG. 5

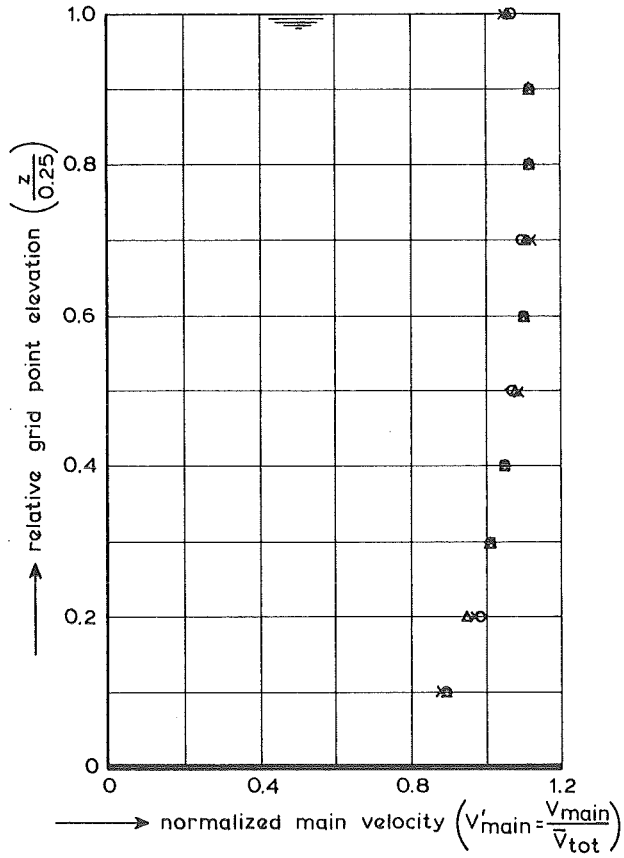

(A) VERTICAL $E_0 3$

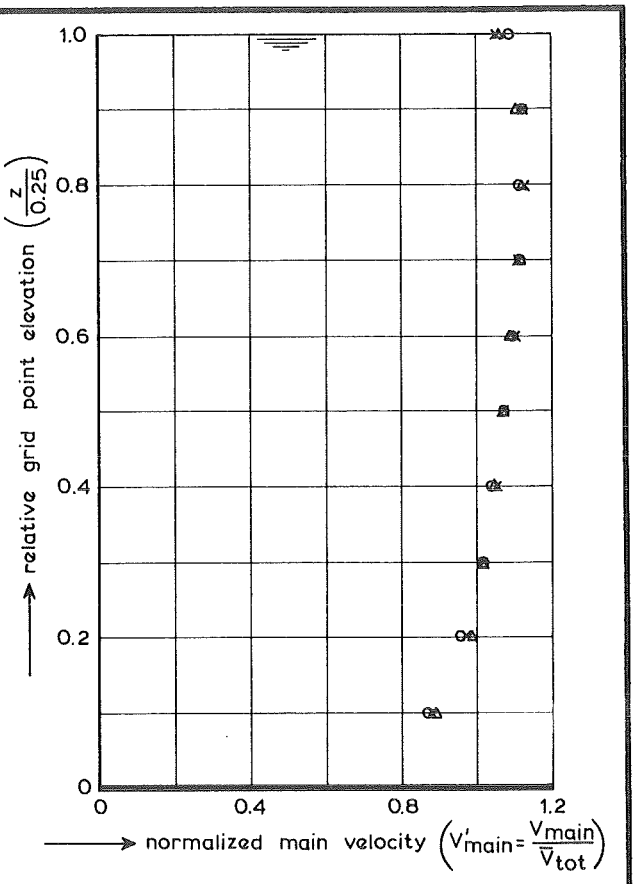

(B) VERTICAL $E_0 7$

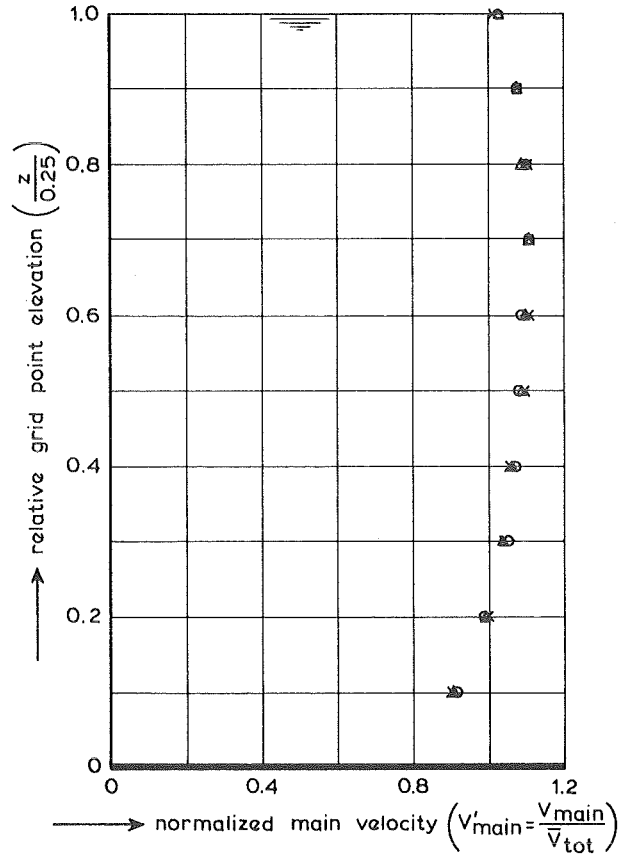

(C) VERTICAL $E_0 11$

x test T1-1
o test T1-2
Δ test T1-3

VERTICAL DISTRIBUTION OF THE NORMALIZED MAIN VELOCITY DURING TAIL-GATE TEST	T1-1,2,3	
DELFT HYDRAULICS LABORATORY/DELFT UNIVERSITY OF TECHNOLOGY	R657/M1415	FIG. 6

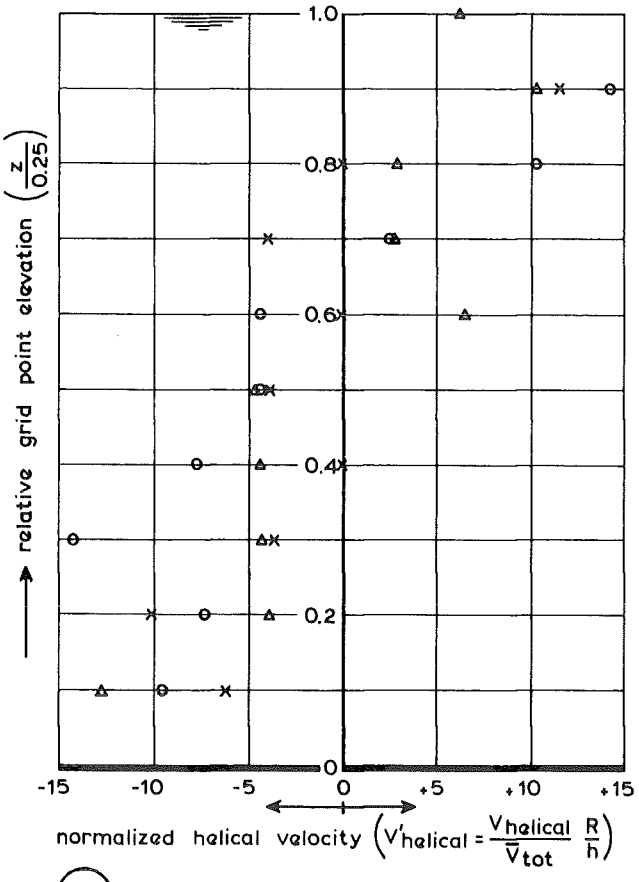

(A) VERTICAL $E_0 3$

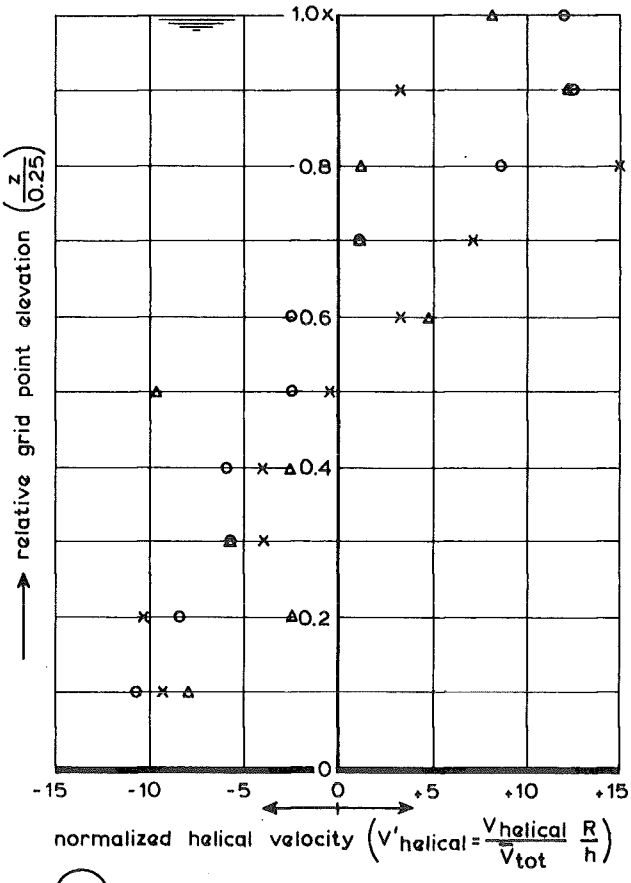

(B) VERTICAL $E_0 7$

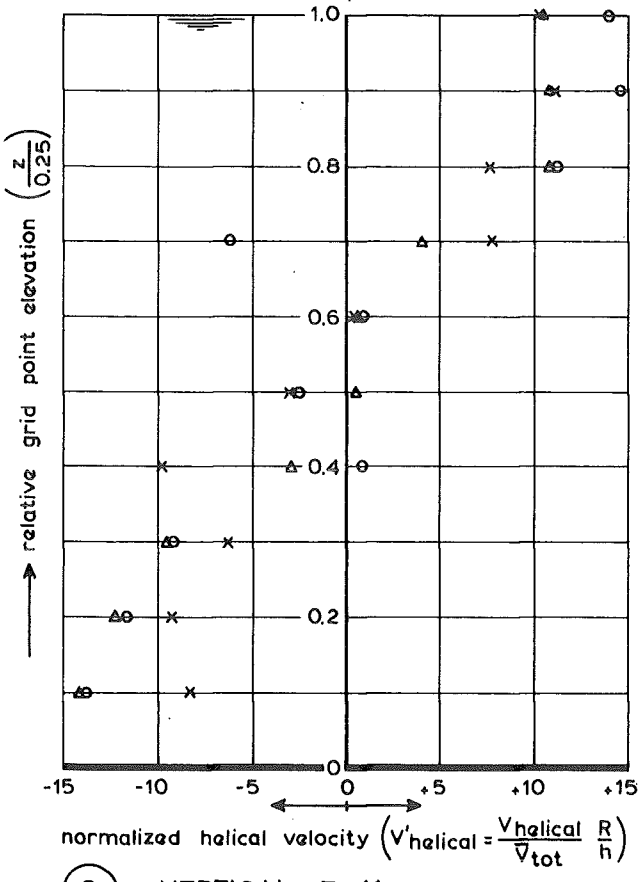

(C) VERTICAL $E_0 11$

x test T1-1
o test T1-2
Δ test T1-3

VERTICAL DISTRIBUTION OF THE NORMALIZED HELICAL VELOCITY DURING TAIL-GATE TEST

T1-1,2,3

DELFT HYDRAULICS LABORATORY/DELFT UNIVERSITY OF TECHNOLOGY | R657/M1415 | FIG. 7

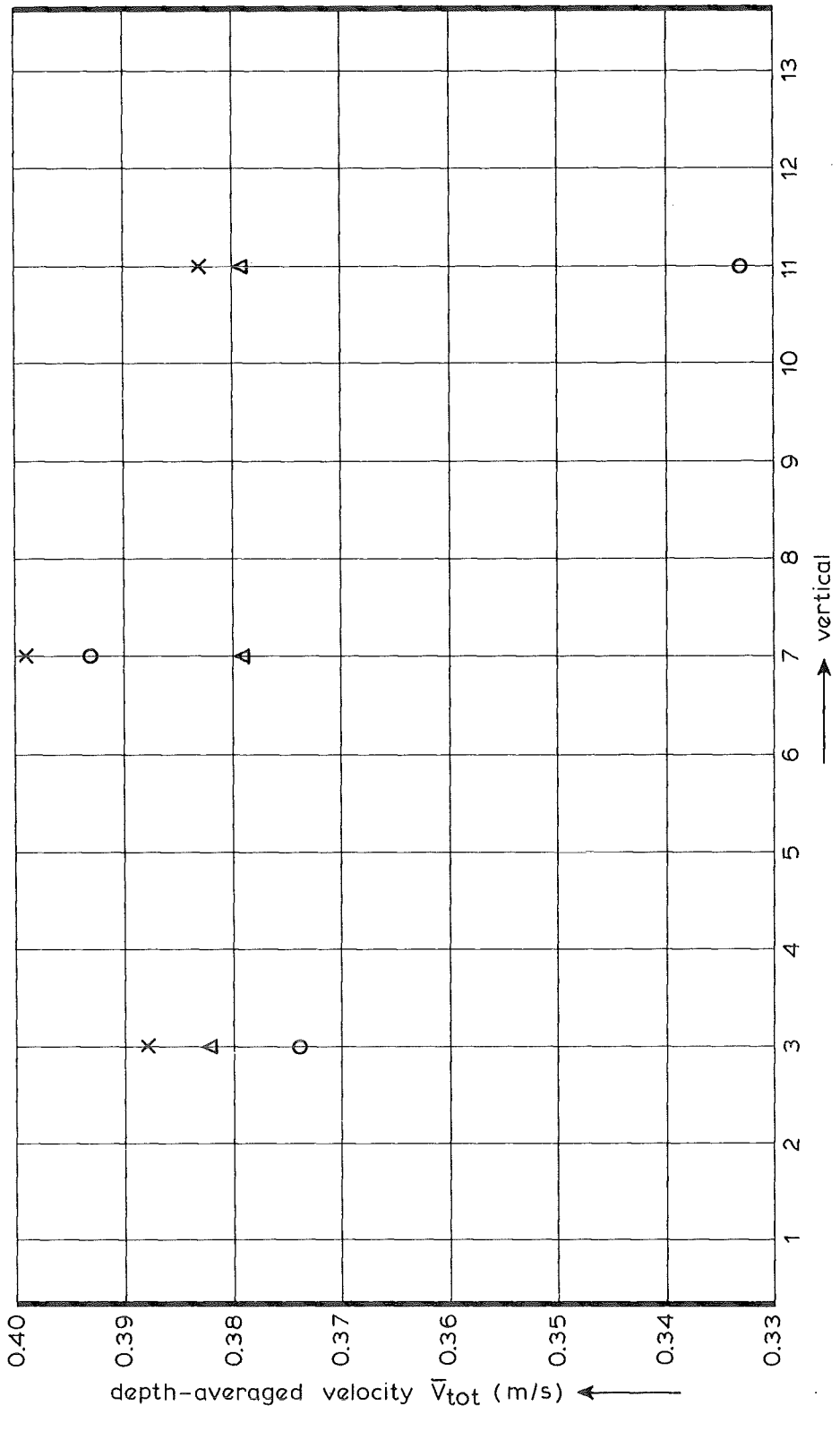

DEPTH-AVERAGED VELOCITY IN SECTION E_0 DURING TAIL-GATE TEST	T1 - 1,2,3	
DELFT HYDRAULICS LABORATORY/DELFT UNIVERSITY OF TECHNOLOGY	R657/M1415	FIG. 8

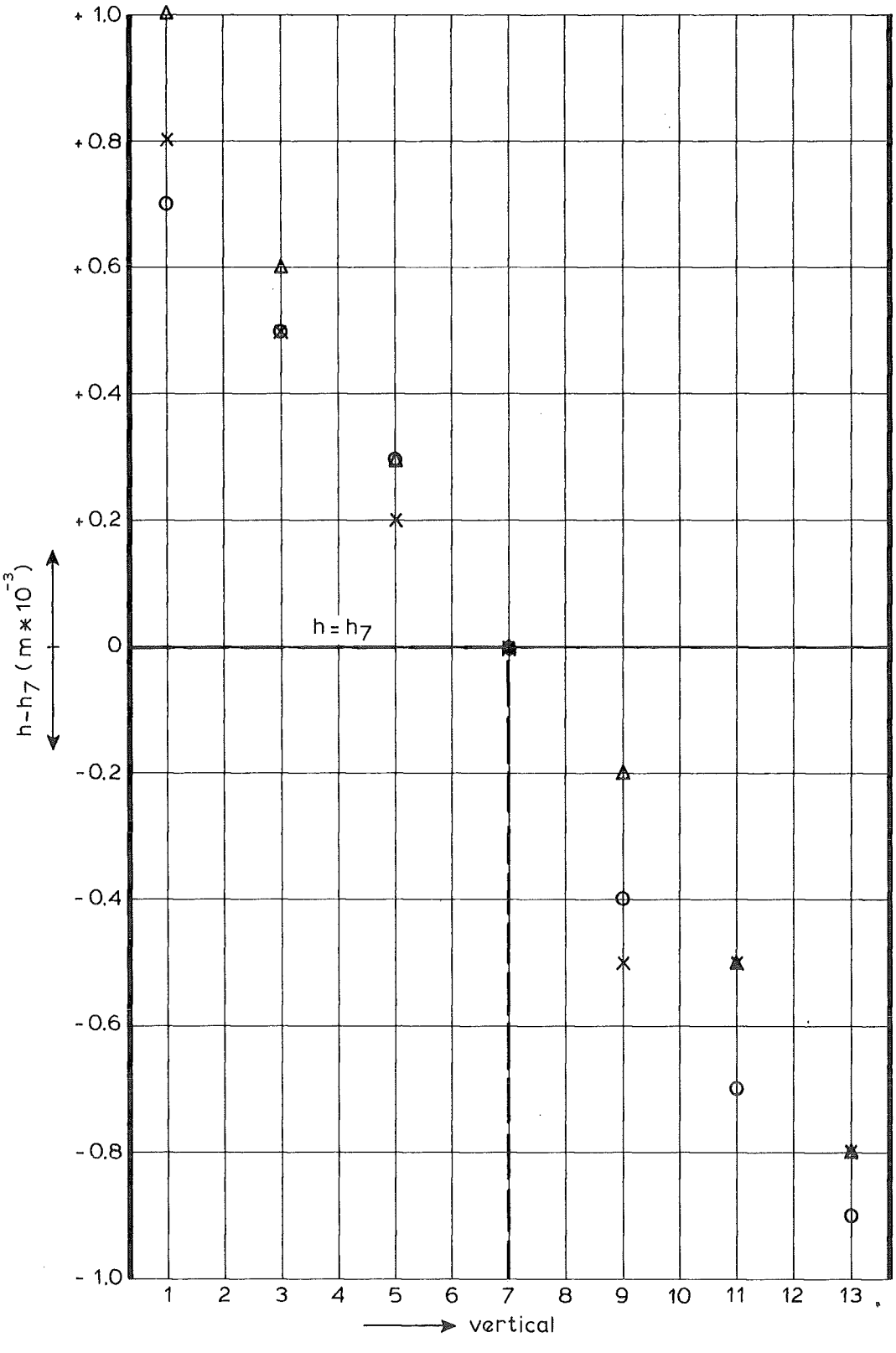

WATER SURFACE ELEVATION IN SECTION E_0 DURING TAIL-GATE TEST

T1-1,2,3

DELFT HYDRAULICS LABORATORY/DELFT UNIVERSITY OF TECHNOLOGY | R657/M1415 | FIG. 9

VERTICAL DISTRIBUTION OF THE NORMALIZED MAIN VELOCITY IN THE CHANNEL AXIS

T2 –1,2

DELFT HYDRAULICS LABORATORY/ DELFT UNIVERSITY OF TECHNOLOGY | R657/M1415 | FIG. 10

991-tt

VERTICAL DISTRIBUTION OF THE NORMALIZED MAIN VELOCITY IN CROSS-SECTION D0

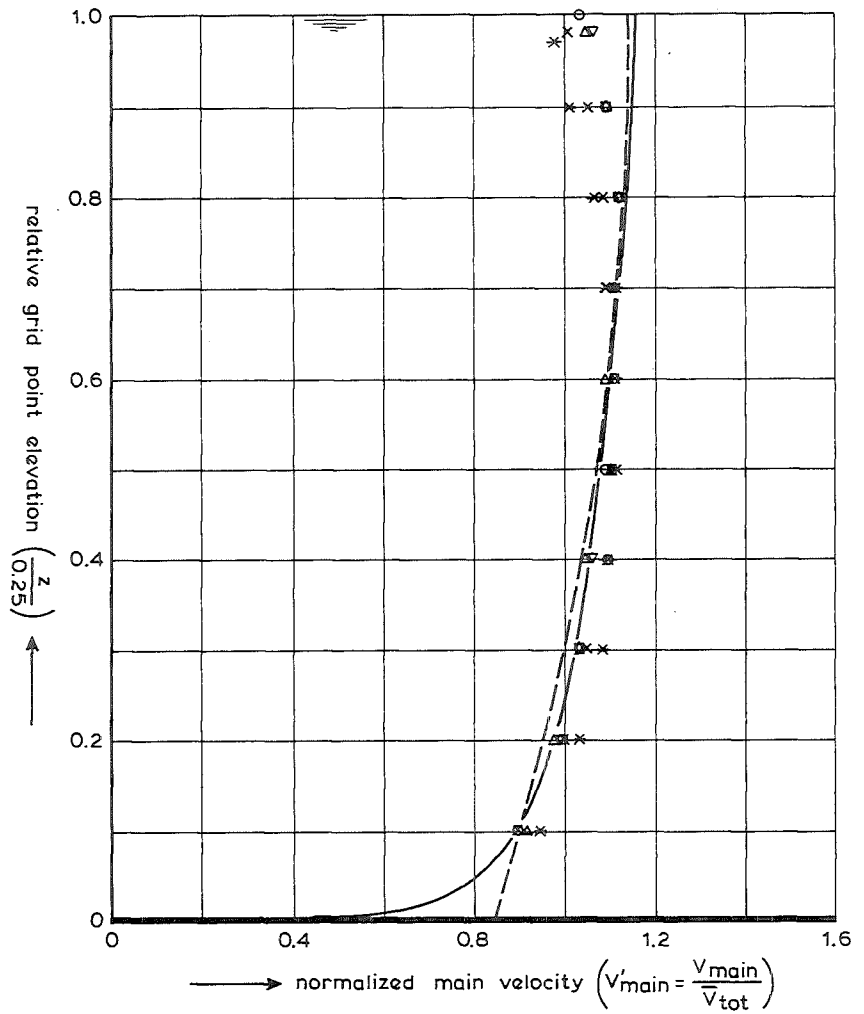

A Q = 0.610 m³/s

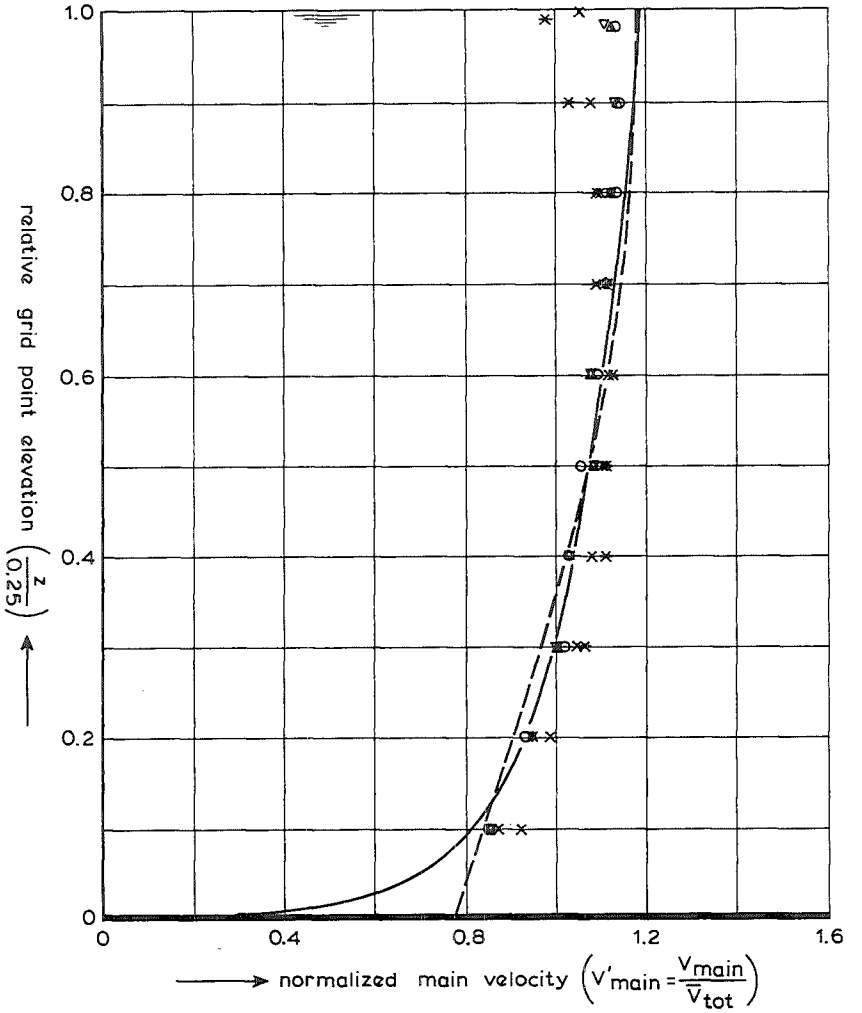

B Q = 0.305 m³/s

theory : ——— logarithmic law
– – – parabolic law

× vertical D0 1
o vertical D0 4
Δ vertical D0 7
▽ vertical D0 10
✳ vertical D0 13

DELFT HYDRAULICS LABORATORY / DELFT UNIVERSITY OF TECHNOLOGY | R657/M1415 | FIG. 11 | T2 – 1,2

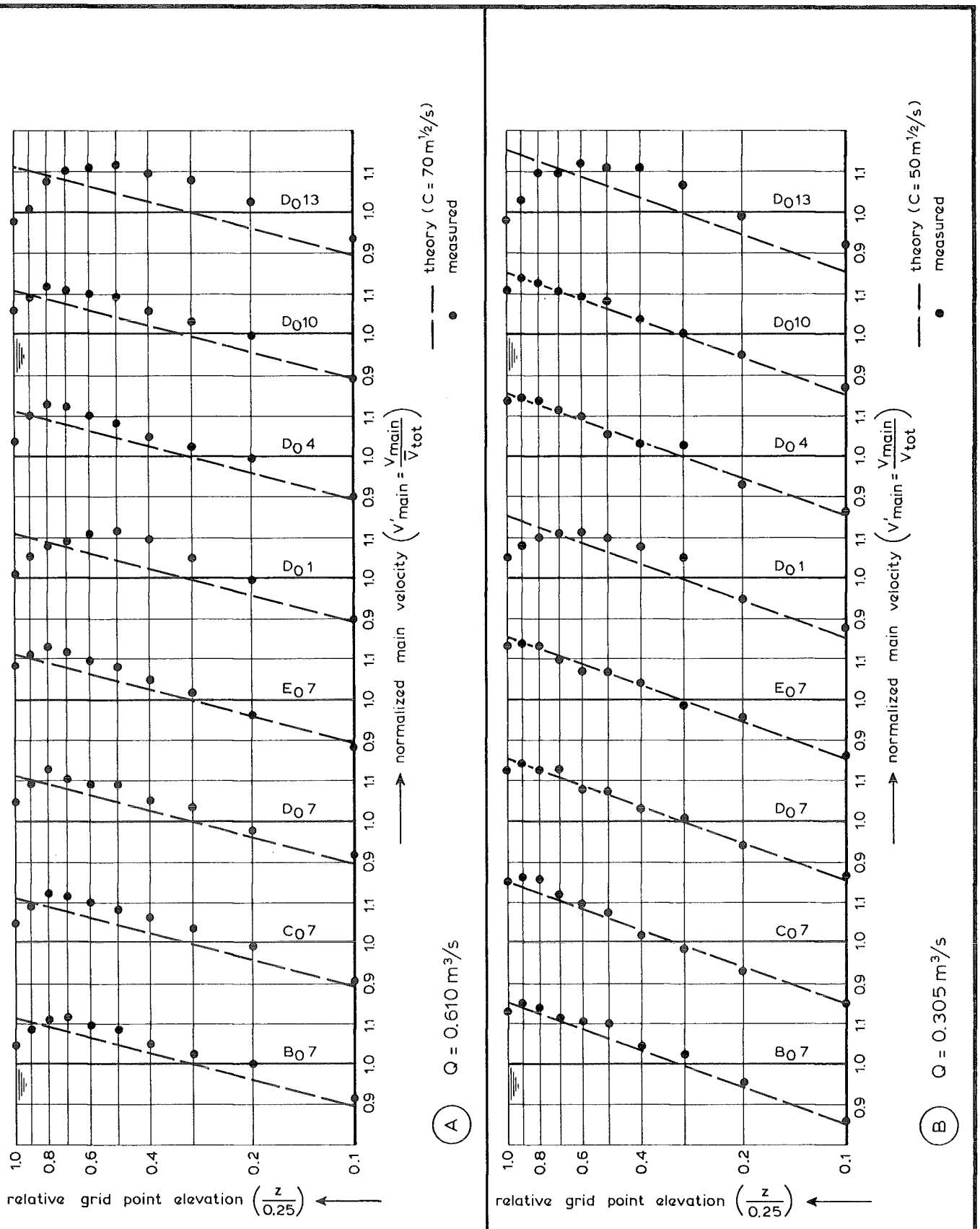

SUMMARY OF THE VERTICAL DISTRIBUTIONS OF THE NORMALIZED MAIN VELOCITY

T2-1,2

DELFT HYDRAULICS LABORATORY/DELFT UNIVERSITY OF TECHNOLOGY | M657/M1415 | FIG. 12

VERTICAL DISTRIBUTION OF THE NORMALIZED HELICAL VELOCITY IN THE CHANNEL AXIS

T2-1,2

DELFT HYDRAULICS LABORATORY/DELFT UNIVERSITY OF TECHNOLOGY | R657/M1415 | FIG. 13

11-1969

VERTICAL DISTRIBUTION OF THE NORMALIZED HELICAL VELOCITY IN CROSS-SECTION D_0

T2-1,2

DELFT HYDRAULICS LABORATORY/DELFT UNIVERSITY OF TECHNOLOGY | R657/M1415 | FIG. 14

SUMMARY OF NORMALIZED HELICAL VELOCITIES IN CROSS-SECTIONS C_o, D_o AND E_o

T2-1,2

DELFT HYDRAULICS LABORATORY/DELFT UNIVERSITY OF TECHNOLOGY | R657/M1415 | FIG. 15

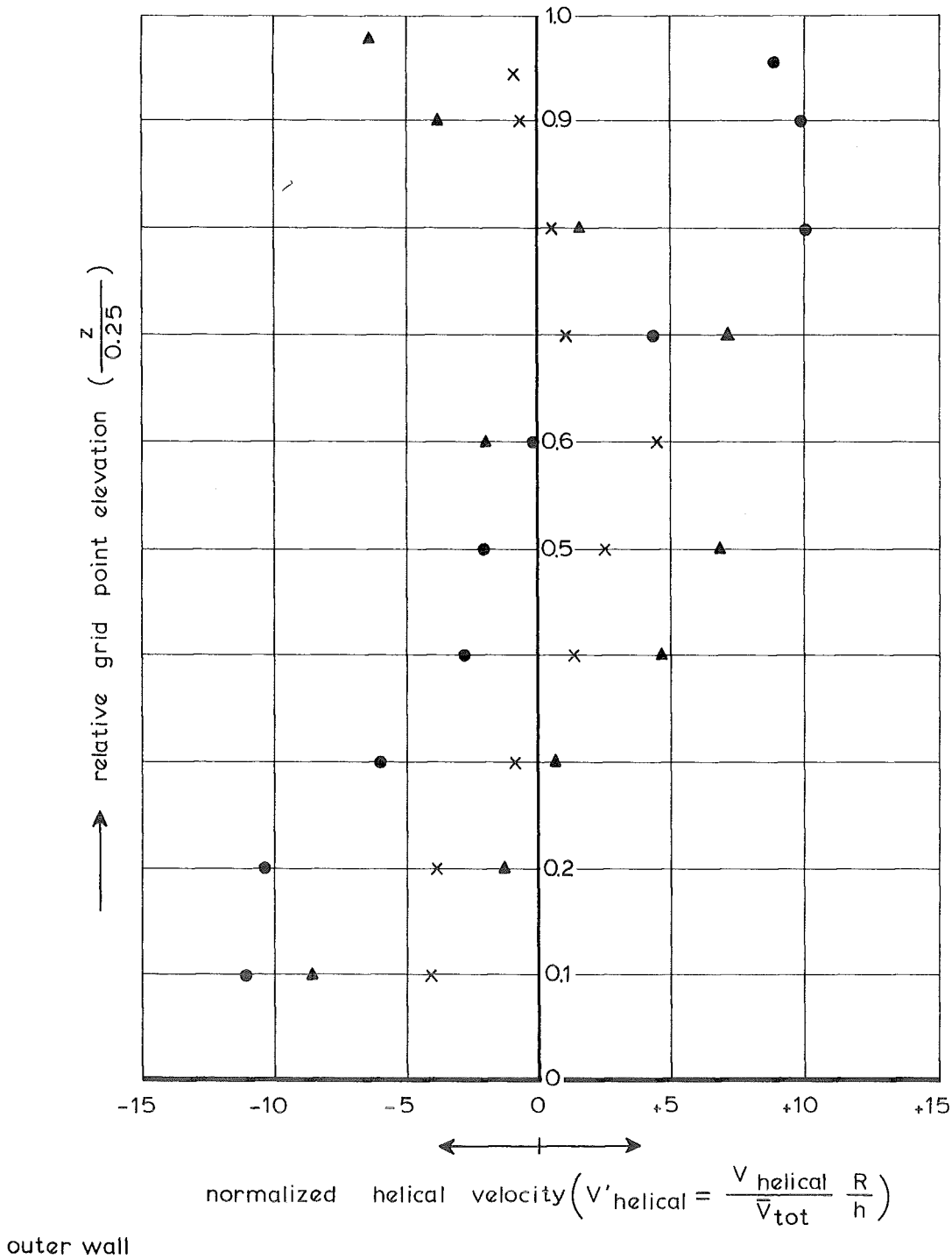

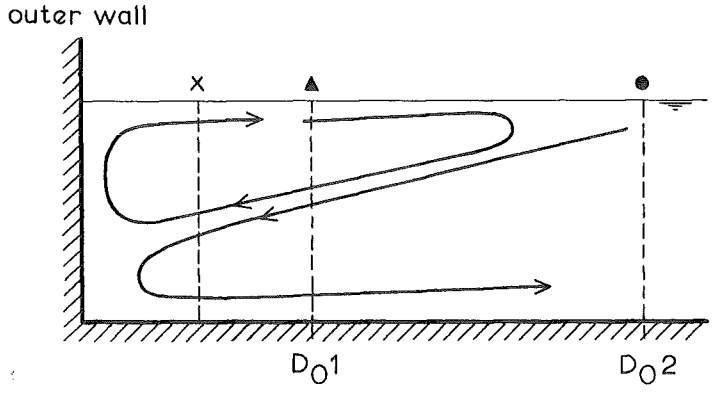

x at 0.15 m from the wall
▲ vertical $D_0 1$
● vertical $D_0 2$

VERTICAL DISTRIBUTION OF THE NORMALIZED HELICAL VELOCITY NEAR THE OUTER WALL IN CROSS - SECTION D_0	T 2 - 3	
DELFT HYDRAULICS LABORATORY/DELFT UNIVERSITY OF TECHNOLOGY	R657/M1415	FIG. 16

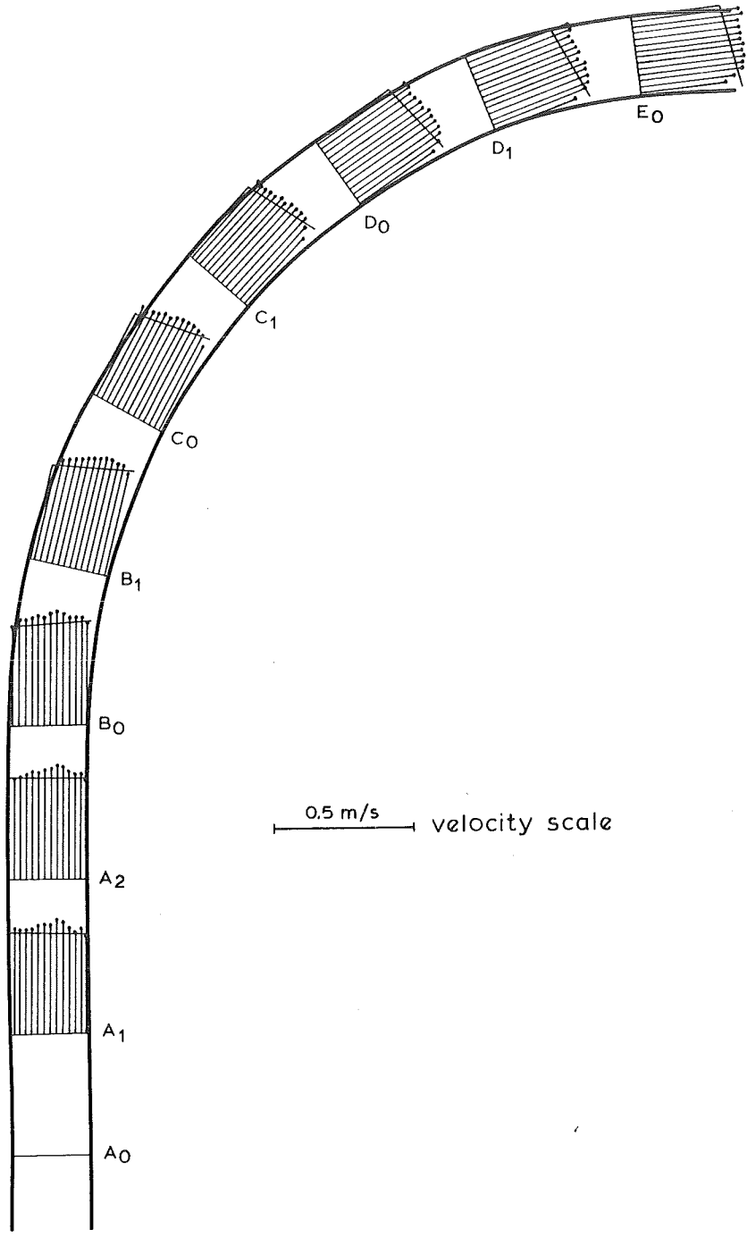

(A) Q = 0.610 m /s

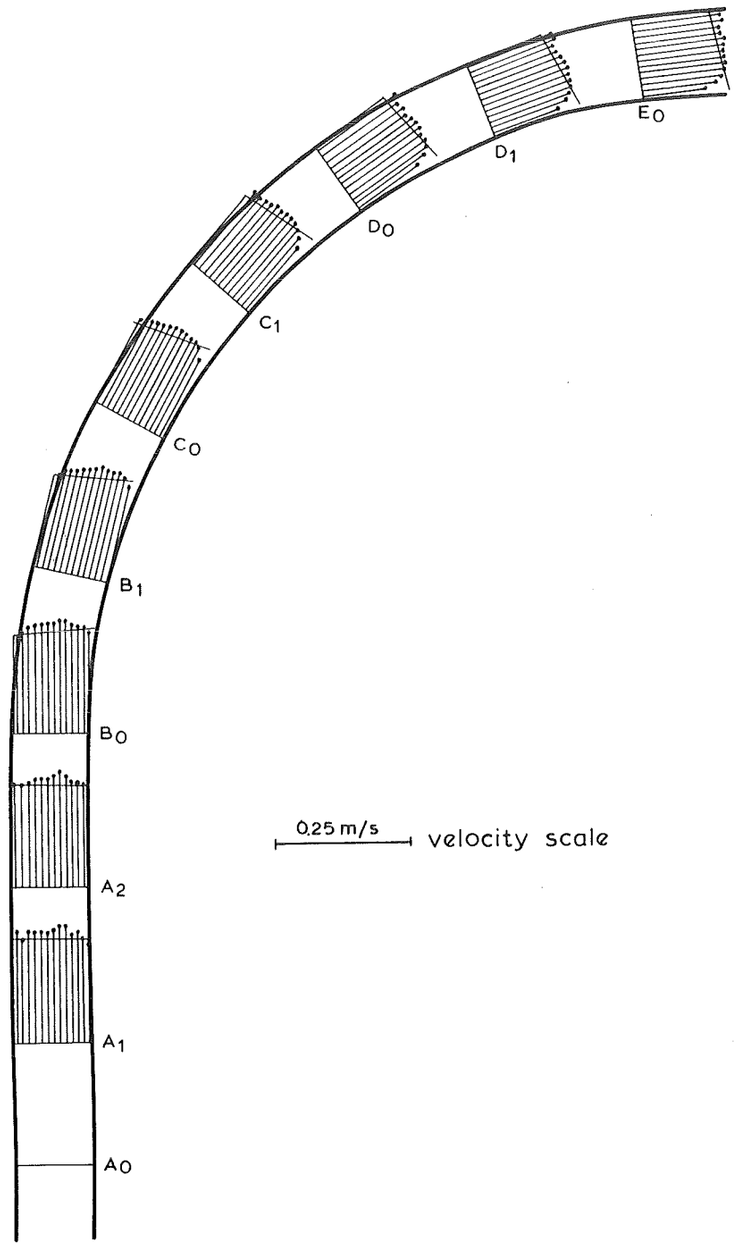

(B) Q = 0.305 m /s

..... measured

——— computed

DEPTH-AVERAGE VELOCITY FIELD	T 3 – 1,2	
DELFT HYDRAULICS LABORATORY/DELFT UNIVERSITY OF TECHNOLOGY	R 657/M1415	FIG. 17

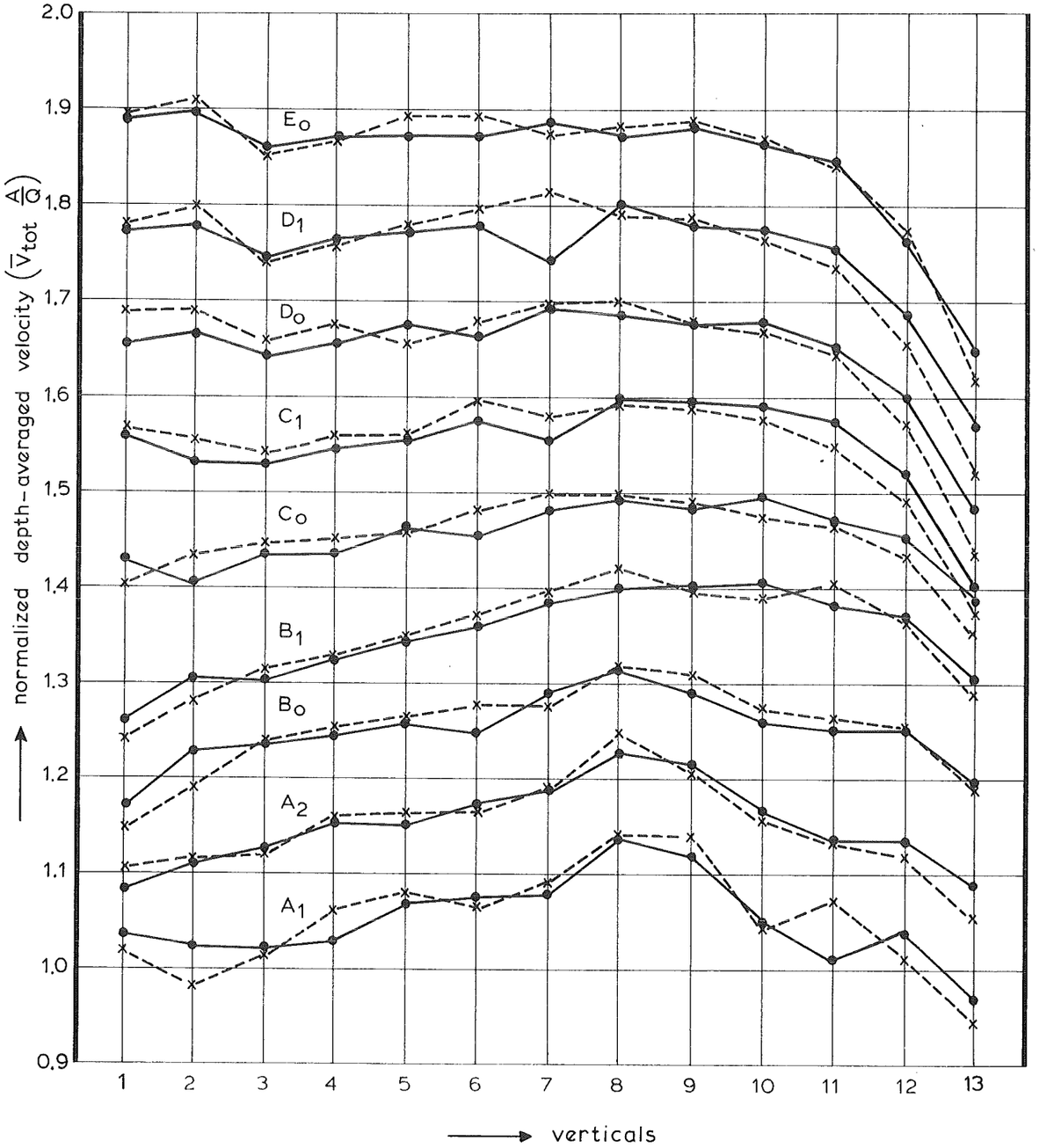

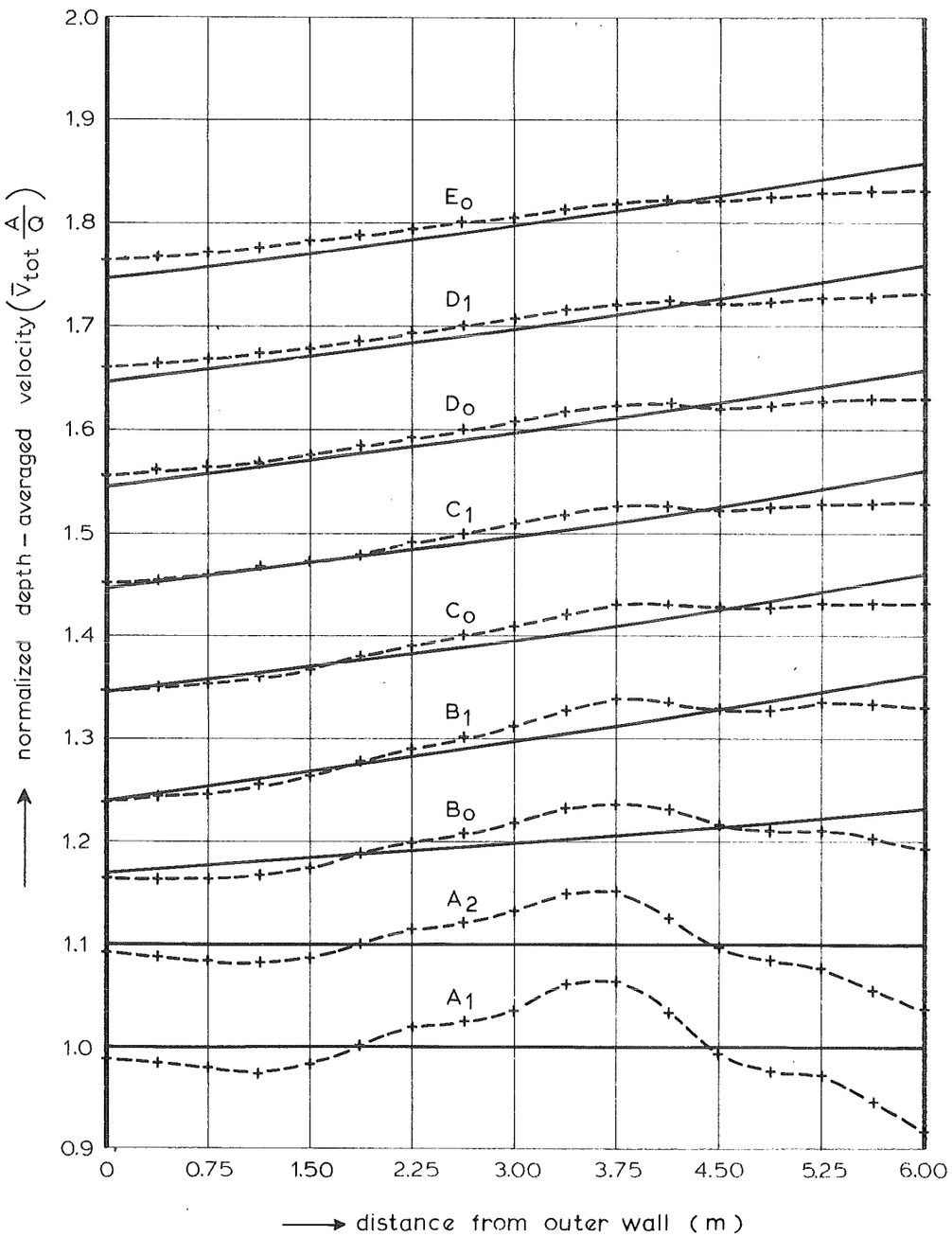

(A) MEASURED

—●—●—●— Q = 0.610 m³/s

—x—x—x— Q = 0.305 m³/s

(B) COMPUTED

——— both discharges Q = 0.610 m³/s
Q = 0.305 m³/s

—+—+— Q = 610 m³/s with measured inflow condition

The velocity scale is given for cross-section A_1
In the subsequent cross-sections the values of $\bar{V}_{tot}\frac{A}{Q}$ have been raised by 0.1

COMPARISON BETWEEN THE DEPTH-AVERAGED VELOCITIES	T 3 - 1,2	
DELFT HYDRAULICS LABORATORY/DELFT UNIVERSITY OF TECHNOLOGY	R 657/M1415	FIG. 18

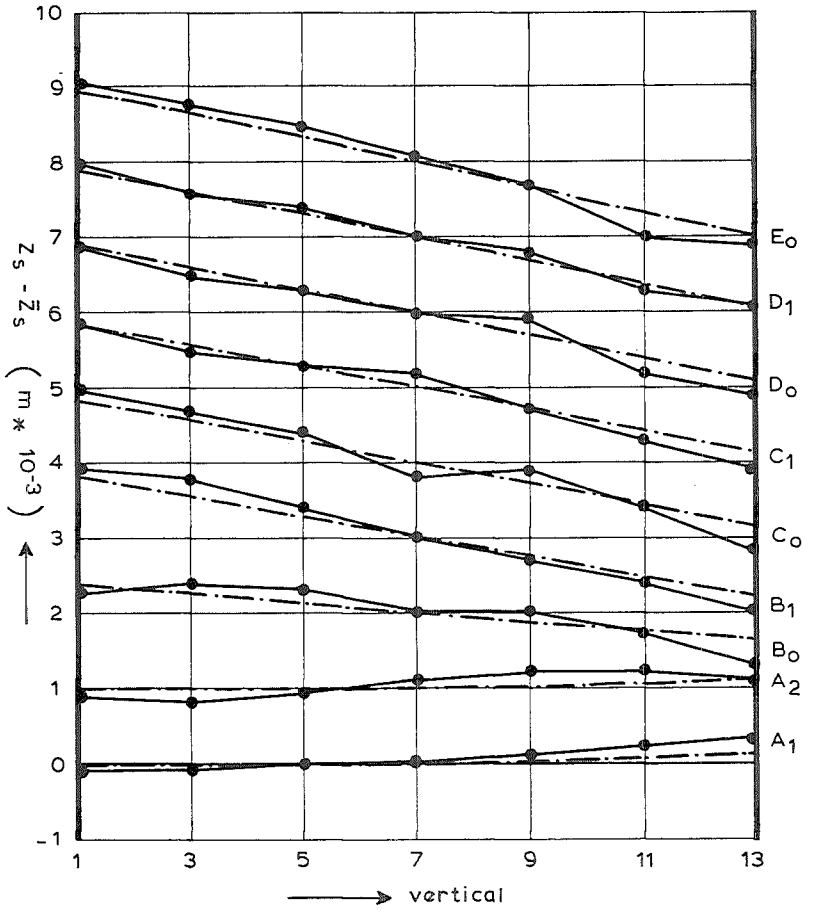

(A) Q = 0.610 m³/s

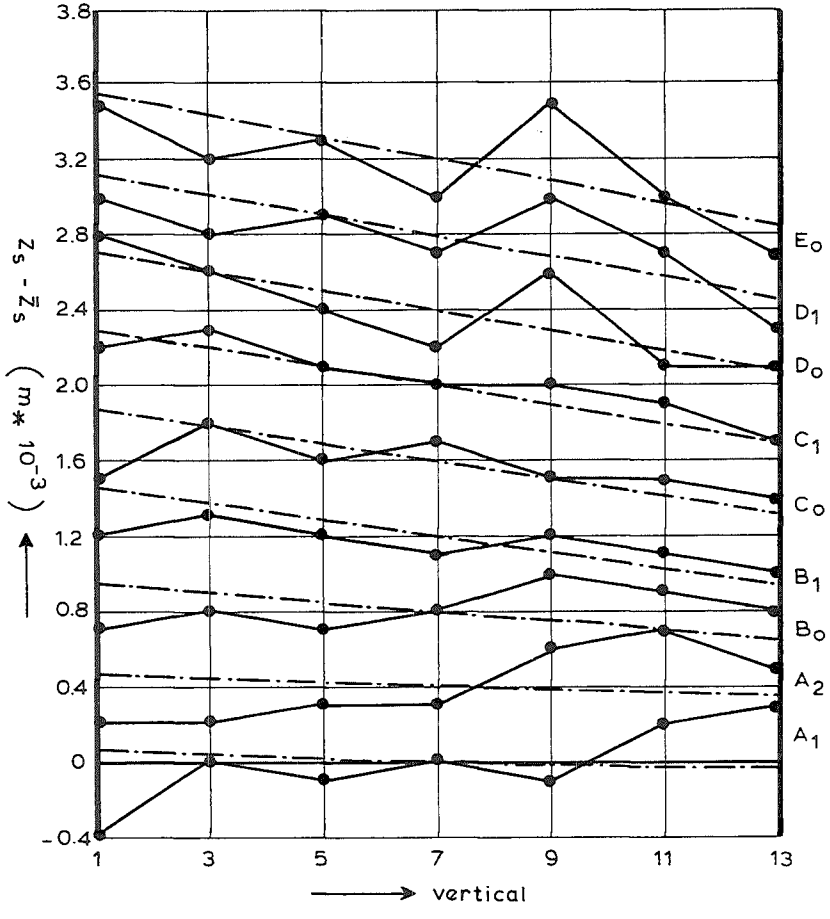

(B) Q = 0.305 m³/s

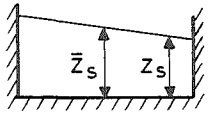

measured

computed

The surface elevation scale is given for cross-section A_1 In the subsequent cross-sections the values of $Z_s - \bar{Z}_s$ have been raised by 10^{-3} m and $0.4 * 10^{-3}$ m respectively

WATER SURFACE ELEVATION

T 4 - 1,2

DELFT HYDRAULICS LABORATORY/DELFT UNIVERSITY OF TECHNOLOGY R 657/M1415 FIG. 19

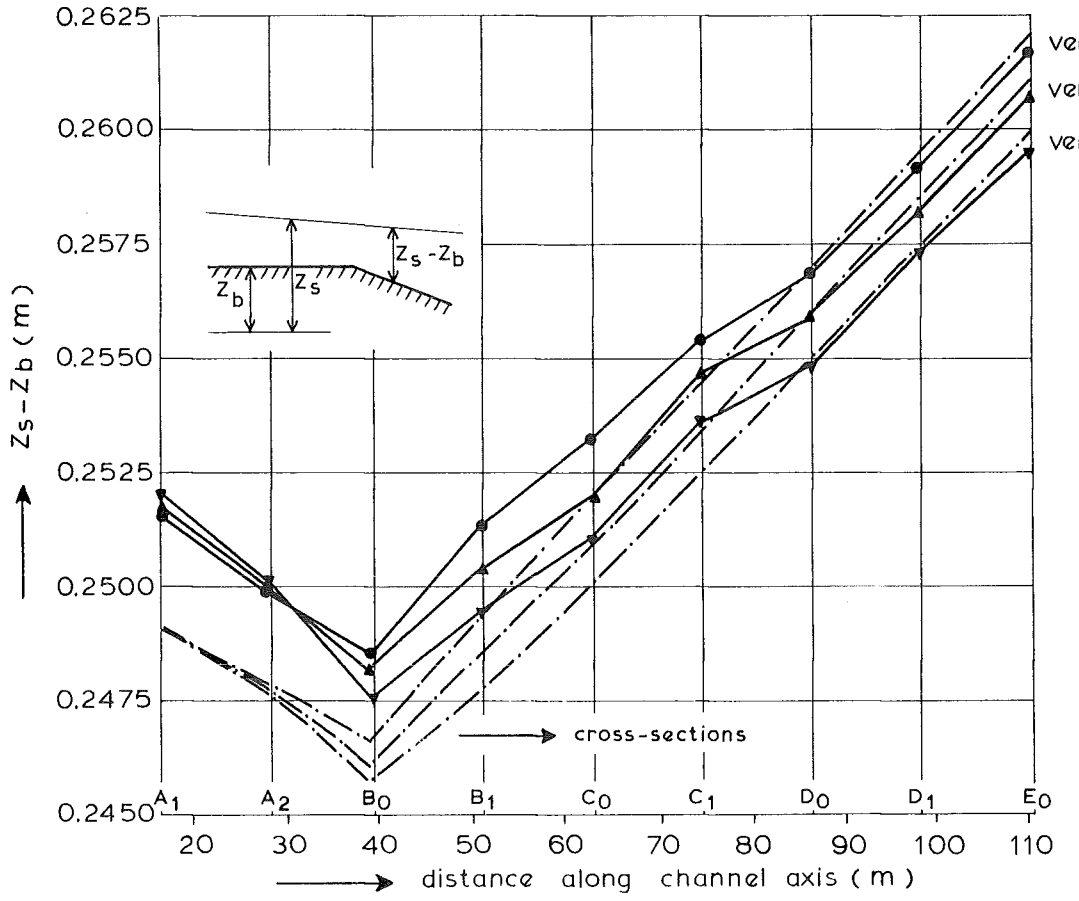

(A) Q = 0.610 m³/s

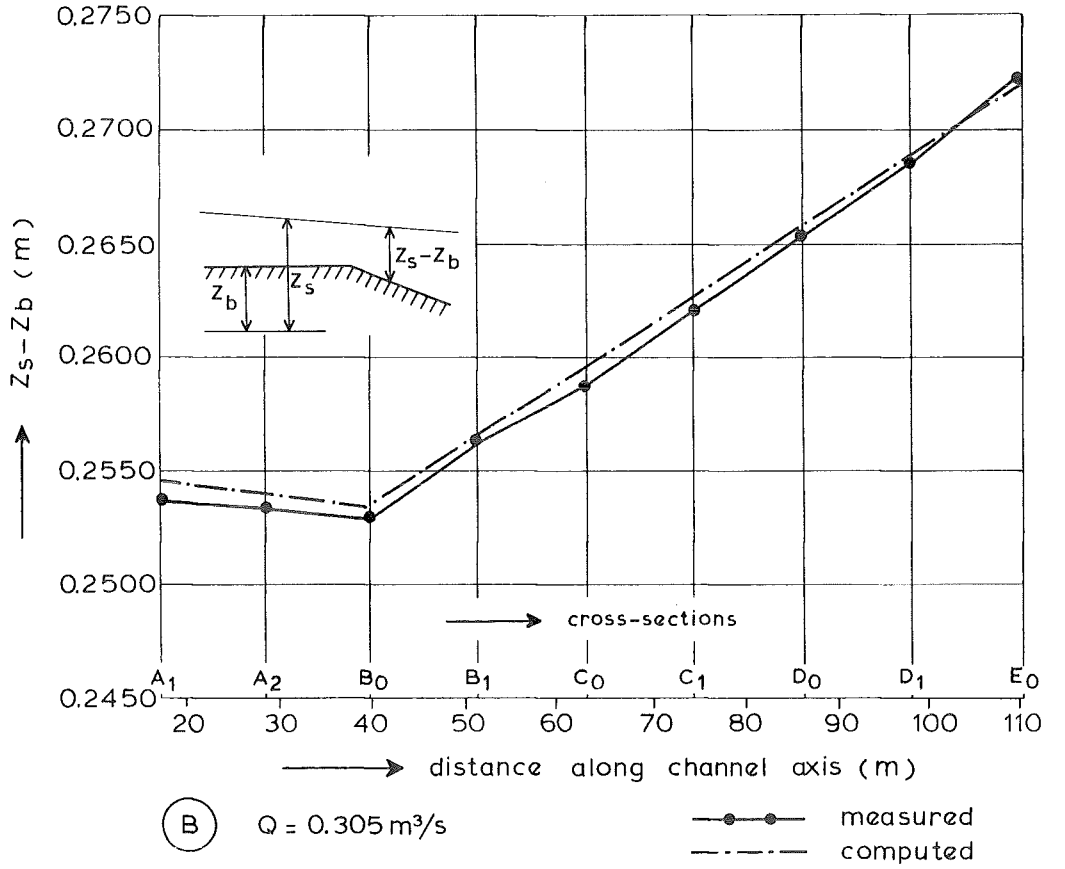

(B) Q = 0.305 m³/s

measured
computed

DEPTH OF FLOW

T4 - 1,2

DELFT HYDRAULICS LABORATORY/DELFT UNIVERSITY OF TECHNOLOGY | R657/M1415 | FIG. 20

ERRORS IN THE NORMALIZED VELOCITIES

DELFT HYDRAULICS LABORATORY/DELFT UNIVERSITY OF TECHNOLOGY | R657/M1415 | FIG. 21